

Swift J1644+57 gone MAD: the case for dynamically-important magnetic flux threading the black hole in a jetted tidal disruption event

Alexander Tchekhovskoy^{1*}, Brian D. Metzger², Dimitrios Giannios³, and Luke Z. Kelley⁴

¹Center for Theoretical Science, Jadwin Hall, Princeton University, Princeton, NJ 08544, USA; Center for Theoretical Science Fellow

²Department of Physics, Columbia University, 538 West 120th Street, 704 Pupin Hall, New York, NY 10027, USA

³Department of Physics, Purdue University, 525 Northwestern Avenue, West Lafayette, IN 47907, USA

⁴Astronomy Department, Harvard University, 60 Garden Street MS 10, Cambridge, MA 02138, USA

Accepted . Received ; in original form

ABSTRACT

The unusual transient Swift J1644+57 likely resulted from a collimated relativistic jet, powered by the sudden onset of accretion onto a massive black hole (BH) following the tidal disruption (TD) of a star. However, several mysteries cloud the interpretation of this event, including (1) the extreme flaring and ‘plateau’ shape of the X-ray/ γ -ray light curve during the first $t - t_{\text{trig}} \sim 10$ days after the γ -ray trigger; (2) unexpected rebrightening of the forward shock radio emission at $t - t_{\text{trig}} \sim$ months; (3) lack of obvious evidence for jet precession, despite the misalignment typically expected between the angular momentum of the accretion disk and BH; (4) recent abrupt shut-off in the jet X-ray emission at $t - t_{\text{trig}} \sim 1.5$ years. Here we show that all of these seemingly disparate mysteries are naturally resolved by one assumption: the presence of strong magnetic flux Φ_{\bullet} threading the BH. Just after the TD event, Φ_{\bullet} is dynamically weak relative to the high rate of fall-back accretion \dot{M} , such that the accretion disk (jet) freely precesses about the BH axis = our line of site. As \dot{M} decreases, however, Φ_{\bullet} becomes dynamically important, leading to a state of ‘magnetically-arrested’ accretion (MAD). MAD naturally aligns the jet with the BH spin, but only after an extended phase of violent rearrangement (jet wobbling), which in Swift J1644+57 starts a few days before the γ -ray trigger and explains the erratic early light curve. Indeed, the *entire* X-ray light curve can be fit to the predicted power-law decay $\dot{M} \propto t^{-\alpha}$ ($\alpha \simeq 5/3 - 2.2$) if the TD occurred a few weeks prior to the γ -ray trigger. Jet energy directed away from the line of site, either prior to the trigger or during the jet alignment process, eventually manifests as the observed radio rebrightening, similar to an off-axis (orphan) gamma-ray burst afterglow. As suggested recently, the late X-ray shut-off occurs when the disk transitions to a geometrically-thin (jet-less) state once \dot{M} drops below \sim the Eddington rate. We predict that, in several years, a transition to a low/hard state will mark a revival of the jet and its associated X-ray emission. We use our model for Swift J1644+57 to constrain the properties of the BH and disrupted star, finding that a solar-mass main sequence star disrupted by a relatively low mass $M_{\bullet} \sim 10^5 - 10^6 M_{\odot}$ BH is consistent with the data, while a WD disruption (though still possible) is disfavored. The magnetic flux required to power Swift J1644+57 is much too large to be supplied by the star itself, but it could be collected from a quiescent ‘fossil’ accretion disk that was present in the galactic nucleus prior to the TD. The presence (lack of) of such a fossil disk could be a deciding factor in what TD events are accompanied by powerful jets.

Key words: MHD – black hole physics – gamma-rays: galaxies – X-rays: galaxies – accretion, accretion discs

1 INTRODUCTION

The unusual soft γ -ray/X-ray/radio transient Swift J164449.3+573451 (hereafter Sw J1644+57) has been broadly interpreted as resulting from a relativistic outflow, powered by accretion following the tidal disruption (TD) of a star by a massive

* E-mail: atchekho@princeton.edu (AT)

black hole (BH) (Bloom et al. 2011; Burrows et al. 2011; Levan et al. 2011; Zauderer et al. 2011). Evidence supporting this model includes the rapid onset of Sw J1644+57 and its location at the center of a compact galaxy at redshift $z \approx 0.353$ (Levan et al. 2011). At least until recently, the SED showed two distinct components, which led Bloom et al. (2011) and Burrows et al. (2011) to suggest different sources for the X-ray and radio emission (see also Liu et al. 2012). The X-ray/ γ -ray emission is highly variable, which indicates an origin from relatively small radii, likely from a location internal to the jet itself (although see Socrates 2012). Figure 1 shows that the emission was particularly variable for the first ~ 10 days after the *Swift*/BAT trigger, t_{trig} (though roughly constant in a time-averaged sense), after which point undergoing a power-law decline,

$$L_X \propto (t - t_{\text{trig}})^{-\alpha}, \quad (1)$$

with $\alpha \sim 5/3$, consistent with the rate of fall-back accretion in simple TD models (e.g. Rees 1988; Lodato et al. 2009; Guillochon & Ramirez-Ruiz 2012; Stone et al. 2012; although see Cannizzo et al. 2011). The X-ray flux has recently abruptly dropped by more than two orders of magnitude, indicating that the jet has apparently ‘shut off’ approximately 500 days after the initial trigger (Zauderer et al. 2012). The total isotropic X-ray energy radiated to date is $\sim 5 \times 10^{53}$ ergs.

In contrast to the X-ray emission, brightness temperature constraints place the radio emission from Sw J1644+57 at much larger radii, suggesting that it instead results from synchrotron emission powered by the shock interaction between the relativistic jet and the surrounding circumnuclear medium (Giannios & Metzger 2011; Zauderer et al. 2011; Metzger et al. 2012; Berger et al. 2012; Wiersema et al. 2012; Zauderer et al. 2012). By modeling the observed radio emission based on the first several weeks of data, Metzger, Giannios & Mimica (2012) (hereafter MGM12) derived values for the bulk Lorentz Factor $\Gamma_j \approx 10$, opening angle $\theta_j \sim 1/\Gamma_j \sim 0.1$, and beaming fraction $f_b \approx 3 \times 10^{-3}$ of the jet which are remarkably similar to those of AGN jets. Berger et al. (2012) (hereafter B12) presented updated radio light curves of Sw J1644+57, which showed a distinct *rebrightening* starting at $t - t_{\text{trig}} \sim 1$ month and peaking on a timescale of several months. This behavior is surprising since the emission is significantly brighter than expected if the blast wave were evolving with a relatively constant energy, as would be expected if the instantaneous jet power tracked the X-ray light curve. B12 proposed that this large additional energy results from slower material catching up to the forward shock at late times. Regardless of its interpretation, however, the radio rebrightening clearly indicates the jet structure (angular or temporal) is more complex than those commonly and successfully applied to normal gamma-ray burst afterglows (Panaitescu & Kumar 2002; Cao & Wang 2012; Liu et al. 2012).

The discovery of a jetted TD event presents several theoretical mysteries. Relativistic jets from AGN are thought to result from magnetic, rather than hydrodynamic, collimation and acceleration (e.g. Rees et al. 1982).¹ If the jet energy derives from the Penrose-Blandford-Znajek process, then the total jet power is given

by (Tchekhovskoy et al. 2010):

$$\begin{aligned} P_j &= \frac{\kappa c}{16\pi r_g^2} \Phi_\bullet^2 \omega_H^2 f(\omega_H) \\ &= 1.2 \times 10^{47} \Phi_{\bullet,30}^2 M_{\bullet,5}^{-2} \omega_H^2 f(\omega_H) \text{ erg s}^{-1}, \\ &= 0.5 \times 10^{47} \Phi_{\bullet,30}^2 M_{\bullet,5}^{-2} \text{ erg s}^{-1}, \end{aligned} \quad (2)$$

$$(3)$$

where $\kappa \approx 0.045$, $r_g = GM_\bullet/c^2$ is BH gravitational radius; $\Phi_\bullet = 10^{30} \Phi_{\bullet,30}$ cgs is the magnetic flux threading the hole; $M_\bullet = M_{\bullet,5} 10^5 M_\odot$ is the BH mass; $\omega_H = a/[1 + (1 - a^2)^{1/2}]$ is dimensionless angular frequency of BH horizon (equals unity for a maximally spinning BH); and $f(\omega_H) = 1 + 0.35\omega_H^2 - 0.58\omega_H^4$ is a high-spin correction, while the normalization in the third line has been calculated for $a = 0.9$.

Sw J1644+57 radiated $\sim 2 \times 10^{53}$ ergs over the first ~ 10 days after the trigger, corresponding to an average isotropic X-ray luminosity $L_X^{\text{trig}} \sim 2 \times 10^{47}$ erg s⁻¹. The total (true) jet power during this interval was thus $P_j^{\text{trig}} = 2(f_b \epsilon_{\text{bol}} \epsilon_X^{-1}) L_X \approx 10^{46} (f_b \epsilon_{\text{bol}} \epsilon_X^{-1} / 0.03)$ erg s⁻¹, where $\epsilon_b \sim \text{few}$ is a bolometric correction; $\epsilon_X < 1$ is the jet radiative efficiency; and the factor of 2 accounts for the other jet beamed away from Earth. Equation (3) shows that in order to explain P_j^{trig} , the required magnetic flux $\Phi_{\bullet,30} \sim M_{\bullet,5}$ for $a = 0.9$, is several orders of magnitude larger than that through a typical main sequence star (Bloom et al. 2011). In §5.2 we discuss possible alternative sources of magnetic flux, such as could be supplied by a pre-existing quiescent accretion disk.

Regardless of its origin, the high luminosity of Sw J1644+57 requires a large magnetic flux. In fact, at least two independent arguments suggest that such magnetic flux was actually present. First, note that a significant fraction of the mass of the disrupted star, and hence of its magnetic flux or that of a quiescent disk, is accreted on the characteristic fall-back time t_{fb} [eq. (12)] of the most tightly bound tidal debris (e.g. Ulmer 1999; Strubbe & Quataert 2009). Equation (3) would thus naively imply that the average jet power should be constant, or rising, at times $t \gg t_{\text{fb}}$, in contradiction to the observed power-law decline in the X-ray luminosity. Using 3D GRMHD simulations, Tchekhovskoy et al. (2011) have shown that if the magnetic flux Φ_\bullet is sufficiently high, then magnetic forces impede accretion onto the BH, causing the flow to enter a ‘magnetically-arrested’ (MAD; e.g. Narayan et al. 2003; Igumenov 2008). MAD flows achieve a quasi-steady state as the result of 3D instabilities, which allow matter to slip past the field lines towards the BH. This process regulates the jet power [eq. (3)] to be proportional to the BH feeding rate, $P_j \propto \dot{M}$ [eq. (17)]. Hence, the fact that the late-time jet power in Sw J1644+57 faithfully tracks the expected rate of fall-back accretion $\dot{M} \propto t^{-\alpha}$ is only naturally understood if the flow is in a magnetically-arrested state.

Additional evidence for a strong magnetic flux is related to the mystery raised by Stone & Loeb (2012), who noted that in general a TD jet should precess if it is pointed along the angular momentum axis of the accretion disk.² Lack of clear evidence³ for large-scale jet precession in Sw J1644+57 thus requires either a set of highly unlikely circumstances, such as an unphysically low BH spin or

¹ One theoretical objection to a hydrodynamic jet is the drag due to Compton cooling (e.g. Phinney 1982), which could in principle, however, be substantially reduced in the case of a TDE due to the lack of a previously-existing broad line region.

² A disk-aligned jet is expected if outflows from the disk are sufficiently powerful to direct the jet on large scales, as is likely if the accretion rate is highly super-Eddington.

³ Saxton et al. (2012) and Lei et al. (2012) argue that the ‘dipping’ behavior and other quasi-periodic features observed in the X-ray light curve of Sw J1644+57 are due to the jet precession/nutation. However, the high duty cycle of observed emission would still require a relatively small (and hence fine-tuned) inclination between the BH spin and stellar orbit ($\lesssim 10 - 20^\circ$).

near-perfect alignment between the angular momentum of the BH and the original orbit of the disrupted star (Stone & Loeb 2012), or some mechanism for aligning the angular momentum of the disk with the BH spin. In fact, recent numerical simulations by McKinney et al. (2012a) (hereafter MTB12a) show that such an alignment between the disk and BH spin axis *can* occur due to MHD forces, but only if the strength of the magnetic field threading the BH is similar to that required for MAD accretion. If such an alignment process occurred in Sw J1644+57, then *the lack of observed precession also provides indirect evidence for a strong magnetic flux.*

In this paper, we present a new physical scenario for Sw J1644+57 which addresses the seemingly disparate mysteries raised above, including the shape of the X-ray/ γ -ray light curve; lack of jet precession; and late radio rebrightening. We show that all of these features are naturally expected given a single assumption: the presence of a strong magnetic flux threading the BH. We begin in §2 with some basic phenomenological considerations. Then in §3 we overview the timeline of our proposed scenario for Sw J1644+57. In §4 we use our model to constrain the properties of the BH and stellar progenitor. In §5 we discuss our results, including the nature of the disrupted star (§5.1); the origin of the magnetic flux (§5.2); the nature and duration of the flaring state (§5.3); the origin of the radio rebrightening (§5.4); and future predictions (§5.5). We present our conclusions in §6. Throughout the paper we use Gaussian-cgs units and set the zero time to the point of disruption, $t_{\text{disr}} = 0$.

2 PHENOMENOLOGICAL CONSIDERATIONS

We begin by discussing the origin of several features in the X-ray and radio light curves of Sw J1644+57 from a phenomenological perspective. Then in §3 we present a more systematic overview of our model.

2.1 Relativistic Jet as the Origin of X-ray Emission

Figure 1 shows the soft X-ray (0.3–10 keV) light curve of Sw J1644+57. Upper limits on the mass of the host galaxy and the observed variability timescale place a rough upper limit of $M_{\bullet} \lesssim 10^7 M_{\odot}$ on the mass of the central BH (e.g. Bloom et al. 2011). The jet luminosity was thus highly super-Eddington over at least the first several days of activity, even after correcting for jet beaming (MGM12). At $t \gtrsim 10$ days, the time-averaged emission follows a power-law decline with temporal index $\alpha \simeq 5/3$ (eq. [1]), similar to the rate of mass fall-back in standard TD scenarios (Rees 1988). This decay rate has been used as evidence that Sw J1644+57 was in fact a TD event, but as we discuss below, it is not clear *a priori* why the jet power should so faithfully track the accretion rate.

2.2 Early Time Light Curve ‘Plateau’

The first ~ 10 days of Sw J1644+57 was characterized by particularly intense flaring (Fig. 1). The luminosity during this period, though variable by several orders of magnitude, was approximately constant on average. Such a ‘plateau’ has no obvious explanation in TD scenarios, but, as we now discuss, it naturally results if the γ -ray trigger was delayed with respect to the time of disruption.

Figure 1 shows that a plateau consistent with the data is reproduced simply by shifting the zero-point of time, even for a purely power-law decay in the assumed flux. In order to reproduce the duration of the plateau and match the predicted accretion rate to

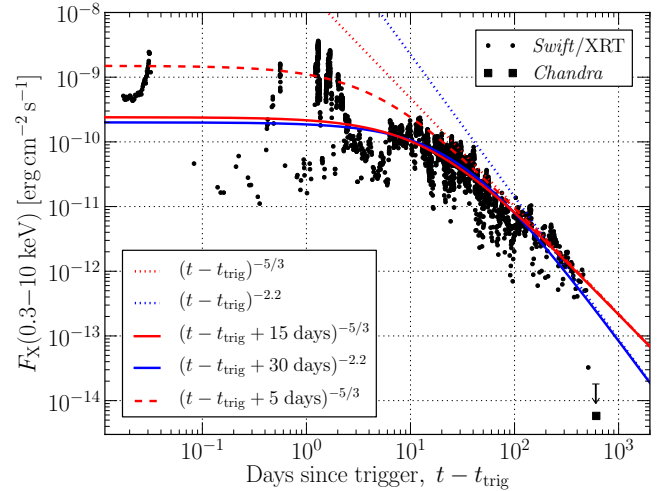


Figure 1. X-ray light curve of Sw J1644+57, as measured by the *Swift* X-ray Telescope (XRT) and *Chandra*. When plotted as a function of time since the γ -ray trigger $t - t_{\text{trig}}$ the average emission shows a ‘plateau-like’ phase lasting for ~ 10 days, which naively appears inconsistent with the predicted power-law decay $\dot{M}_{\text{fb}} \propto (t - t_{\text{disr}})^{-\alpha}$ in the rate of fall-back accretion following a tidal disruption event ($t = t_{\text{disr}}$). However, if the trigger time is delayed with respect to the disruption, then a ‘plateau’-like shape in $F_X(t - t_{\text{trig}})$ is naturally produced (§2.2). The two solid curves show $\dot{M}_{\text{fb}} \propto t^{-\alpha}$ (arbitrary normalization) for complete (red, $\alpha = 5/3$ for trigger time delay $t_{\text{trig}} - t_{\text{disr}} = 15$ days) and partial stellar disruption (blue, $\alpha = 2.2$, $t_{\text{trig}} - t_{\text{disr}} = 30$ days), while the dotted curves show the conventional versions of power-law fits that neglect the trigger time delay. The trigger time delay for the solid lines are chosen to match \dot{M}_{fb} with the the average luminosity of the early plateau phase ($t - t_{\text{trig}} \lesssim 10$ days). If we instead match \dot{M}_{fb} to the ‘envelope’ created in the light curve by the brightest flares, then adopting a shorter trigger time delay is also consistent with the data, e.g., $t_{\text{trig}} - t_{\text{disr}} = 5$ days for a complete disruption (red dashed line, $\alpha = 5/3$). This timescale is consistent with the first evidence for activity from Sw J1644+57 (Burrows et al. 2011; Krimm & Barthelmy 2011; Zauderer et al. 2011) 4 days prior to the first BAT trigger.

the average X-ray flux, we find that a trigger delay $t_{\text{trig}} - t_{\text{disr}} \sim$ weeks-month is required, depending on whether the TD event was a complete ($\alpha \simeq 5/3$) or partial disruption ($\alpha = 2.2$; we discuss this distinction in §3). If we instead fit the ‘envelope’ of X-ray emission set by the brightest flares (a factor ~ 10 times higher flux than the plateau average), then a shorter trigger delay $t_{\text{trig}} - t_{\text{disr}} \sim 5$ days is also consistent with the data (justification of such a possibility is discussed in §4.2.1). There in fact was evidence for jet activity ~ 4 days prior to the *Swift* trigger (on March 28, 2011) as seen in both *Swift*/BAT data (Krimm & Barthelmy 2011; Burrows et al. 2011), as well as inferred by the rise time of the radio emission (Zauderer et al. 2011; MGM12). However, our fits in Figure 1 show that the TD event could have occurred much earlier than this time.

2.3 Jet Activity Prior to Trigger and Radio Rebrightening

What could cause such a long delay before the onset of jet emission? One possibility is that the process of jet formation requires special conditions which only became satisfied at late times after the disruption, such as the accumulation of a critical quantity of magnetic flux (§5.3). It is also possible that the jet *was* active soon after disruption, but that it was initially pointed away from our line of site, as could be expected if the black hole spin and the angular momentum of the fall-back disk were initially misaligned. Even

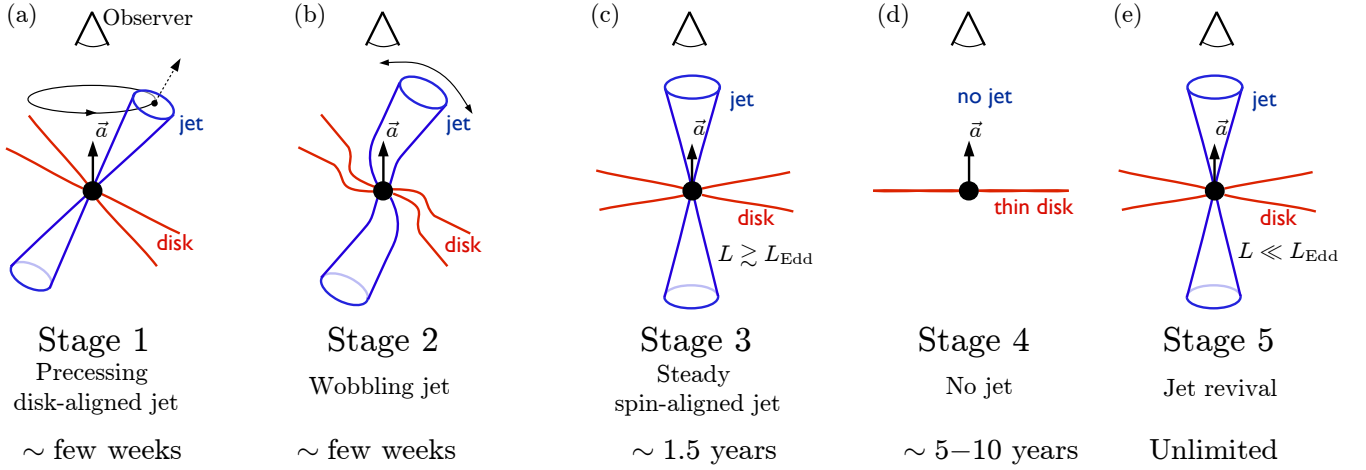


Figure 2. Stages in the proposed model for Sw J1644+57. **[Panel (a)]: Stage 1.** Shortly after the stellar disruption, the magnetic flux threading the BH Φ_* increases, as it is dragged inward by the accreting material. Stellar debris returning to the BH forms a *tilted* accretion disk, with a rotation axis that is misaligned with the BH spin. The latter points towards our line of site (shown as vertical in the figure). At early times, when the mass accretion rate \dot{M} is highest, the magnetic flux Φ_* is not dynamically important. Under these conditions, the disk undergoes precession due to Lense-Thirring torques (Fragile et al. 2007) and the jets point along the disk axis. Their high-energy emission is beamed away from Earth and is not detectable. **[Panel (b)]: Stage 2.** As \dot{M} decreases with time, the magnetic flux eventually becomes dynamically important, leading to a state of magnetically-arrested disk (MAD) (Narayan et al. 2003; Tchekhovskoy et al. 2011). In the MAD state, the magnetic field is sufficiently strong to offset gravitational forces acting on the inner disk and to align the axis of the disk axis (and hence the jets) with the BH spin (so-called “magneto-alignment effect”; MTB12a). However, it takes time for the entire disk and jet to align with the BH spin. As \dot{M} decreases, the BH magnetic flux and jet power $P_j \propto \dot{M}$ also decrease. As excess magnetic flux leaks out of the BH into the disk, MAD encompasses a larger and larger fraction of the disk. During this process, the jet pushes against the disk and wobbles erratically (see movies in MTB12a). As the jet comes in and out of our line of sight, this produces large amplitude variations (“flares”) in lightcurve of Sw J1644+57 during the first $\sim 10^6$ seconds after the trigger (see Fig. 1). **[Panel (c)]: Stage 3.** Once MAD encompasses the entire disk, the disk/jet alignment with the BH spin completes. Since the jet direction points steadily towards Earth, its X-ray emission becomes less variable as it continues to track the rate of fall-back accretion. **[Panel (d)]: Stage 4.** Once \dot{M} decreases below $\sim 30\%$ of the Eddington accretion rate \dot{M}_{Edd} , the disk transitions to a geometrically-thin state and the jet shuts off, producing an abrupt decline in X-ray emission at $t \gtrsim 500$ days. **[Panel (e)]: Stage 5.** At very late times, once the accretion rate drops below a few percent of \dot{M}_{Edd} , the disk will again enter a geometrically-thick regime, and the jet may turn back on, again analogous to state transitions in X-ray binaries. For Sw J1644+57 this ‘jet revival’ is estimated to occur between the years ~ 2016 – 2022 (§5.5).

if the jet eventually fully aligns towards our line of site, it might not be pointed towards us at all times during initial stages in the alignment process (see below).

Although X-ray emission from a misaligned jet is unobservable, it still imparts kinetic energy into the ambient medium surrounding the black hole. Synchrotron radio emission from this off-axis blast-wave would not be visible initially due to relativistic beaming, but could become visible once the ejecta slows to mildly relativistic Lorentz factor $\gamma \sim 2(0.5/\theta_{\text{ma}})$, where θ_{ma} is the angle between the jet and line of sight, normalized to a typical value $\sim 30^\circ$. A blast wave of [isotropic] energy $E^{\text{iso}} = 10^{54} E_{54}$ erg that interacts with an external medium of density $n = 10 n_1 \text{ cm}^{-3}$ (see MGM12, B12 for motivation for these characteristic values) will decelerate to $\gamma = 2$ at a distance $R_{\text{dec}} \approx 2.4 \times 10^{18} (E_{54}/n_1)^{1/3} \text{ cm}$ from the BH. The observer time corresponding to emission from this radius $t_{\text{obs}} \approx R_{\text{dec}}(1 - \beta \cos \theta_{\text{ma}})/\beta c \lesssim 1 \text{ yr}$, for $\theta_{\text{ma}} \lesssim 0.5$. Delayed emission from such an off-axis jet thus provides a possible explanation for the otherwise mysterious radio rebrightening observed to peak ~ 4 months after the onset of Sw J1644+57 (B12; see §5.4 for further discussion).

2.4 Intense Early-Time Flaring Followed by a Steady Decline

Large-amplitude flares in the early γ -ray/X-ray lightcurve of Sw J1644+57 (Fig. 1) could result from geometric effects, such as changes in jet orientation which cause emission to periodically beam in and out of our line of sight. This erratic ‘wobbling’ of the

jets is a natural consequence of the alignment process. Eventually, once the jet direction becomes stable, one of the jets continuously points towards us. This produces relatively steady X-ray emission at late times ($\gtrsim 10$ days), which decays as a power-law in time, reflecting the rate at which stellar debris returns to the BH.

2.5 Jet Shutoff

The X-ray emission from Sw J1644+57 recently declined abruptly at $t \sim 500$ days, after which time the XRT is able to place only upper limits on the flux (Fig. 1). Sw J1644+57 was subsequently detected by *Chandra* at flux nearly 2 orders of magnitude lower than that just prior to the decline (Sbarufatti et al. 2012; Zauderer et al. 2012); however, this residual flux is consistent with it being the high energy extension of the same forward shock synchrotron emission observed at radio frequencies (Zauderer et al. 2012). Such a jet ‘shut off’ may occur once the accretion rate drops below a fraction of the Eddington accretion rate (Zauderer et al. 2012), since after this time the disk becomes geometrically-thin and enters a thermally-dominant accretion state, which are not observed to produce powerful jets (Russell et al. 2011).

3 TIMELINE OF PROPOSED SCENARIO

We now describe the timeline for our proposed scenario for Sw J1644+57, the stages of which are illustrated in Figure 2.

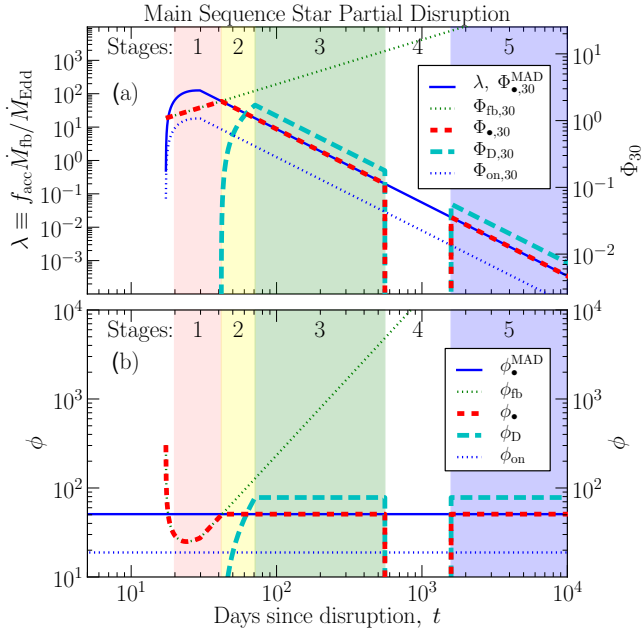


Figure 3. Various quantities as a function of time since disruption, assuming a partial disruption of a MS star and a delay of $t_{\text{trig}} - t_{\text{disr}} = 60$ days between the disruption and the γ -ray trigger (§2.2). Different stages in our model for Sw J1644+57 are indicated with color coding and numbers (§3; see Fig. 2 for a detailed explanation). **[Panel (a)]:** Mass accretion rate $\lambda = \dot{M}/\dot{M}_{\text{Edd}}$ as a fraction of the Eddington accretion rate \dot{M}_{Edd} (blue solid line; left axis), which peaks at $t \approx 1.5t_{\text{fb}} \approx 30$ days and subsequently decays as $\lambda \propto t^{-2.2}$. The same curve (right axis) gives the maximum value of the magnetic flux threading the BH, $\Phi_{\bullet,30}^{\text{MAD}} \propto \lambda^{1/2}$, in units of 10^{30} G cm² (red dashed line). As stellar debris returns to the vicinity of the BH, it drags in magnetic flux from a pre-existing, “fossil” accretion disk (§5.2). This accumulated flux due to the swept-up fossil field increases with time as $\Phi_{\text{fb},30} \propto t^{2/3}$ (green dotted line; eq. 36). At early times, most of this flux ends up on the BH, so $\Phi_{\bullet,30} = \Phi_{\text{fb},30}$ (red dashed line). For our choice of parameters (see below), BH receives a substantial amount of magnetic flux early on, enough to overcome the ram pressure of the infalling gas and produce the jets, $\Phi_{\bullet,30} > \Phi_{\text{on},30}$ (red dashed line lies above blue dotted line). Eventually, the central magnetic flux becomes dynamically-important, i.e., $\Phi_{\bullet,30} \approx \Phi_{\bullet,30}^{\text{MAD}}$ (red dashed line crosses blue solid line). Since the inner disk can only hold $\Phi_{\bullet,30}^{\text{MAD}}$ worth of flux on the hole (Stage 2), the rest leaks out and instead contributes to the disk flux (cyan long-dashed line), i.e. $\Phi_{\text{D},30} = \Phi_{\text{fb},30} - \Phi_{\bullet,30}^{\text{MAD}}$. However, the disk flux eventually also saturates (depending on its radial extent, eq. 43), after which it also tracks the BH magnetic flux (Stage 3). Once the Eddington ratio, λ , falls below a critical value ($\lambda_{\text{cr}} = 0.2$ in this figure) the accretion disk becomes geometrically-thin; the central BH and disk lose their magnetic flux; and the jets shut off (Stage 4). At a much later time, when $\lambda \lesssim 0.02$, the accretion disk becomes geometrically-thick again and produces powerful jets (Stage 5). **[Panel (b)]:** Dimensionless values (eq. 9) of the magnetic flux shown in panel (a). In this figure we have assumed following parameters: BH spin $a = 0.7$; BH mass $M_{\bullet} = 3 \times 10^5 M_{\odot}$; stellar mass $M_{\star} = 0.44 M_{\odot}$; fraction of star accreted by BH $f_{0.4} f_{\text{acc}} = 0.75$; Eddington fraction of the fossil disk $\lambda_{\text{fossil}} = 1.8 \times 10^{-3}$; and $P_j/L_X = f_{\text{beol}} \epsilon_X^{-1} = 0.05$. For computing flux accumulation timescale at early time (eq. 37), we assume disk thickness $h/r = 1$ as expected for a highly super-Eddington flow. Since at later times h/r decreases, for computing jet power we take a single representative value, $h/r = 0.3$.

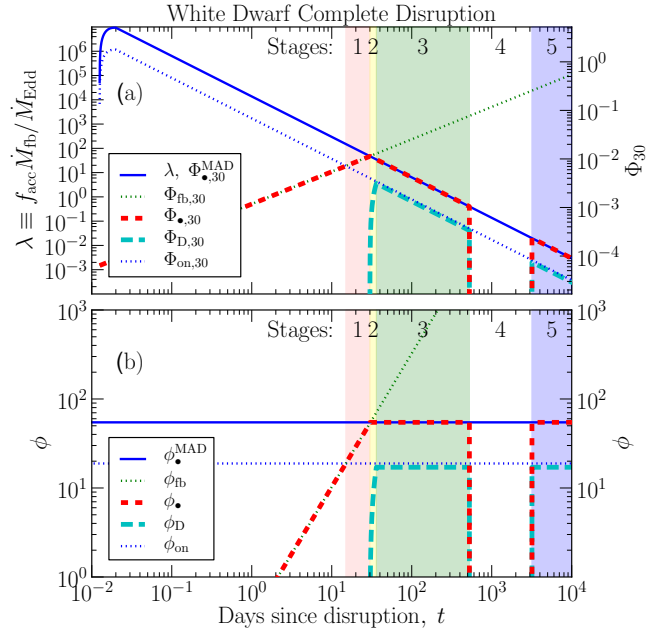


Figure 4. Similar to Figure 3, but shown for the case of a complete disruption of a WD, assuming a disruption-trigger delay of $t_{\text{trig}} - t_{\text{disr}} = 30$ days. Note that unlike the MS star scenario (Fig. 3), the mass accretion rate is highly super-Eddington near the peak ($\lambda \gg 100$), and initially jet production is suppressed (see discussion in §3.2). However, as the mass accretion rate decreases, $\lambda \propto t^{-5/3}$, eventually the magnetic flux becomes sufficiently large to overcome the ram pressure of the accretion flow, $\Phi_{\bullet} > \Phi_{\text{on}} \approx 20$ (red dashed line overtakes blue dotted line), and the jets emerge. After this point, the jet evolution is similar to that described in Figure 3. In this figure, we have assumed the following parameters: $a = 0.87$; $M = 10^4 M_{\odot}$; $M_{\star} = 0.6 M_{\odot}$; $f_{\text{acc}} = 0.54$; $\lambda_{\text{fossil}} = 10^{-8}$; $\lambda_{\text{cr}} = 0.4$; and $f_{\text{beol}} \epsilon_X^{-1} = 0.003$.

3.1 Stage 0: Tidal Disruption and Flux Accumulation

A star of mass $M_{\star} = m_{\star} M_{\odot}$ and radius $R_{\star} = r_{\star} R_{\odot}$ is tidally disrupted by a BH of mass $M_{\bullet} = 10^5 M_{\odot}$ if its pericenter radius R_p lies within the tidal radius $R_t \approx R_{\star} (M_{\bullet}/M_{\star})^{1/3}$. After disruption, approximately half of the star is immediately unbound, while the other half remains marginally bound and is placed on highly elliptic orbits, with the most tightly bound material falling back on a characteristic timescale (Stone et al. 2012)

$$t_{\text{fb}} \approx 17.3 \text{ d } M_{\bullet,5}^{1/2} m_{\star}^{-1} r_{\star}^{3/2}. \quad (4)$$

The fall-back accretion rate \dot{M}_{fb} peaks (at $t_{\text{peak}} \approx 1.5t_{\text{fb}}$; Ulmer 1999) at a characteristic value

$$\dot{M}_{\text{fb,peak}} \approx \frac{\alpha - 1}{2/3} \frac{M_{\star}}{3t_{\text{fb}}} \approx 2 \times 10^{26} \text{ g s}^{-1} \frac{\alpha - 1}{2/3} M_{\bullet,5}^{-1/2} m_{\star}^2 r_{\star}^{-3/2}, \quad (5)$$

or in terms of the Eddington accretion rate $\dot{M}_{\text{Edd}} \equiv L_{\text{Edd}}/0.1c^2$,

$$\frac{\dot{M}_{\text{fb,peak}}}{\dot{M}_{\text{Edd}}} \approx 4 \times 10^3 \frac{\alpha - 1}{2/3} M_{\bullet,5}^{-3/2} m_{\star}^2 r_{\star}^{-3/2}, \quad (6)$$

and subsequently decays as a power law

$$\dot{M}_{\text{fb}} \approx \dot{M}_{\text{fb,peak}} \left(\frac{t}{t_{\text{fb}}} \right)^{-\alpha} \quad (7)$$

where $\alpha = 5/3$ for a complete disruption and $\alpha = 2.2$ for a partial disruption (Guillochon & Ramirez-Ruiz 2012; Figs. 3, 4). Until recently (e.g. Ulmer 1999; Strubbe & Quataert 2009), TD models

predicted that t_{fb} and $\dot{M}_{\text{fb,peak}}$ should depend also on the impact parameter $\beta \equiv R_t/R_p$ in addition to the stellar and BH properties; however, recent numerical (Guillochon & Ramirez-Ruiz 2012) and analytic (Stone et al. 2012) work has shown that these estimates were made on the faulty assumption that the energy distribution of the disrupted stellar material is frozen-in at pericenter instead of the tidal radius.

Matter falls back and circularizes to form an accretion disk at the radius

$$R_{\text{circ}} \simeq 2R_p = 2R_t\beta^{-1} \simeq 430r_*m_*^{-1/3}M_{\bullet,5}^{-2/3}\beta^{-1}r_g, \quad (8)$$

accreting soon thereafter. When the accretion rate is super-Eddington at early times, the disk may be prone to outflows driven by radiation pressure (e.g. Ohsuga et al. 2005; Strubbe & Quataert 2009), in which case the accretion rate reaching the BH is less than \dot{M}_{fb} .

If the magnetic flux responsible for powering the jet in Sw J1644+57 originates from the star itself, then a substantial fraction of the total flux is accumulated on the relatively short fall-back time $t \lesssim t_{\text{fb}}$ (eq. [4]). However, flux accumulation can last significantly longer if the field is swept up from a quiescent fossil disk by the infalling debris (in which case $\Phi_\bullet \propto (t/t_{\text{fb}})^{2/3}$; §5.2). On timescales $t \gtrsim t_{\text{fb}}$ the jet power $P_j \propto \Phi_\bullet^2$ [eq. (3)] thus either saturates to a constant value [stellar flux], or increases as $P_j \propto (t/t_{\text{fb}})^{4/3}$ [fossil disk]. In what follows, we express the flux in a dimensionless form,

$$\phi_\bullet \equiv \frac{\Phi_\bullet}{(\dot{M}r_g^2c)^{1/2}} \approx 30\Phi_{\bullet,30} \left(\frac{\dot{M}}{\dot{M}_{\text{fb,peak}}} \right)^{-1/2} M_{\bullet,5}^{-3/4} m_*^{-1} r_{\star}^{3/4}, \quad (9)$$

that quantifies its dynamical importance in relation to the accreting gas, where $r_g \equiv GM_\bullet/c^2$. Figures 3 and 4 show the time evolution of the Φ_\bullet and ϕ_\bullet in our model for Sw J1644+57, based on two scenarios for the disrupted star (§4.1).

3.2 Stage 1: Precessing Disk-Aligned Jet (Fig. 2a).

In general the angular momentum of the initial stellar orbit and fall-back accretion disk will not be aligned with the spin of the BH. Such tilted, geometrically-thick accretion disks undergo precession due to Lense-Thirring torques, and their jets are also expected to precess (Fig. 2a). Though expected, evidence for precession is not obviously present in the light curve of Sw J1644+57 (Stone & Loeb 2012; although see Saxton et al. 2012; Lei et al. 2012). This mystery is resolved if we postulate that our line of site is aligned with the BH spin axis (§2), such that the emission from the tilted jet is beamed away from us and hence is not initially detectable.

Because the magnetic field is dynamically weakest relative to the accretion flow (ϕ_\bullet is smallest) when the accretion rate is highest $\dot{M} \sim \dot{M}_{\text{fb,peak}}$ (eq. [9]), the magnetic flux does not appreciably influence the disk inclination at these early times. This allows for a phase of jet precession as described above.

At even earlier times, however, when $\phi_\bullet \lesssim \phi_{\text{on}} \approx 20$, the ram pressure of the quasi-spherical accretion flow (as expected for super-Eddington accretion) is so high that it can stifle jet formation altogether (Komissarov & Barkov 2009). Since $\phi_\bullet \propto t^{2/3}$ if $\Phi_\bullet = \text{constant}$, (eq. 9; assuming $\dot{M}_{\text{fb}} \propto t^{-\alpha}$) this limits the duration of Stage 1 to $\sim 4^{-2/\alpha} t_{\text{MAD}} \sim (1/\text{few}) t_{\text{MAD}}$, where t_{MAD} is the onset of MAD accretion (start of Stage 2), which occurs when $\phi_\bullet^{\text{MAD}} \sim 50$. The possibly substantial duration of this early jet smothering phase is illustrated by Figure 4, which shows the time evolution of ϕ_\bullet in the case of a tidally-disrupted WD. In this case, the disruption itself happens on a timescale of \sim tens of minutes, but Stage 1 begins

only at $t \sim 10$ days. Also note that depending on how fast magnetic flux is accumulated, Stage 1 could be even briefer. If $\phi_\bullet \gtrsim \phi_\bullet^{\text{MAD}}$ at peak accretion, then the jet will enter the ‘wobbling’ stage described next essentially from its onset.

3.3 Stage 2: MAD Onset, Erratic Wobbling Jet (Fig. 2b).

As \dot{M} decreases from its peak value, $\phi_\bullet \propto \dot{M}^{-1/2}$ (eq. [9]) increases and the magnetic field becomes increasingly important dynamically. Once ϕ_\bullet exceeds a critical value $\phi_\bullet^{\text{MAD}} \sim 50$ (depending weakly on BH spin; eq. [13]), the field is sufficiently strong to feed-back on the accreting gas, leading to a state of ‘magnetically-arrested disk’ accretion, or MAD (Narayan et al. 2003; Tchekhovskoy et al. 2011; McKinney et al. 2012b).

The strong magnetic flux also acts to orient the rotational axis of the inner accretion disk/jet with the BH spin axis (MTB12a). This realignment does not, however, happen instantaneously, nor is it clean. The jets undergo a period of vigorous rearrangement during which they ram against the accretion disk, partially obliterate it, and intermittently punch holes through the disk as they work to reorient the disk’s angular momentum along BH spin axis (see Fig. 2b). Recent numerical simulations show that during this stage the jets wobble intensely between the orientation of the outer disk axis and the orientation of the BH axis (MTB12a), so that jet emission transiently comes in and out of our line of sight. This jet wobbling state may explain the epoch of intense flaring comprising the first ~ 10 days of the Sw J1644+57 light curve (§2.4).

Alignment between the disk/jet and BH spin completes once sufficient magnetic flux is able to leak out of the immediate vicinity of the BH and new flux is brought in by the infalling debris, such that the *entire* disk (at least out to the circularization radius R_{circ}) becomes magnetically arrested. Depending on R_{circ} , this process requires ϕ_\bullet to increase by a factor of a few, and hence \dot{M} to decrease by a factor of several. In §5.3 we show that this timescale for the entire disk to ‘go MAD’ is broadly consistent with the observed duration of the early flaring state in Sw J1644+57. In Figures 3 and 4 this process is shown by the rising value of the disk flux Φ_D during Stage 2, until it eventually reaches a constant fraction of the BH flux Φ_\bullet at the onset of Stage 3.

3.4 Stage 3: Steady Spin-Aligned Jet (Fig. 2c).

Once the entire disk is magnetically-arrested, the system enters a scale-free MAD solution that depends on just one parameter: the mass accretion rate (Fig. 2c).⁴ The strong centrally-accumulated magnetic field not only aligns the jets along the direction of BH spin axis (§3.3), it also explains why the jet luminosity faithfully tracks mass fallback rate. When ϕ_\bullet is small at early times (Stage 1), the BH flux Φ_\bullet and jet power P_j (eq. [3]) are approximately constant or increase in time (Stage 1), which is inconsistent with the power-law decrease in the X-ray lightcurve of Sw J1644+57 between ~ 10 and ~ 500 days since the trigger (Fig. 1). In contrast, when the central magnetic field is sufficiently strong ($\phi_\bullet \gtrsim \phi_\bullet^{\text{MAD}} \sim 50$; eq. [13]) to be dynamically-important (MAD state), then the magnetic flux Φ_\bullet threading the BH is not determined by initial conditions, but instead by the ram pressure of the accretion flow. Its value regulates such that the jet power $P_j \sim \eta_j \dot{M} c^2$ is a constant fraction $\eta_j \approx 1.3a^2$ of the accretion power (eq. [17]).

⁴ Order unity deviations from self-similarity are possible due to radiation feedback on the accretion flow.

Thus, as the fall-back rate decreases as a power-law in time, so do the jet power and luminosity, as is observed.

Another expected feature of MAD is a stable QPO at a frequency that is 1/4 of BH horizon angular frequency (McKinney et al. 2012b). Reis et al. (2012) detected a potential QPO with period $\tau_{\text{QPO}} \sim 200$ s in the power-law decay portion of the Sw J1644+57 lightcurve, which could also be evidence for MAD. We discuss the constraints implied by this period (§4.2.6) as a part of our analysis in §4.

3.5 Stage 4: No Jet (Fig. 2d).

Once the accretion rate drops below a few tens of per cent of \dot{M}_{edd} , the flow transitions to a geometrically thin disk state, or thermal state, which is not observed (nor theoretically expected) to power a jet (e.g., Fender et al. 2004; Russell et al. 2011). The abrupt decrease in the X-ray flux at $t \sim 500$ days (Fig. 1; by more than two orders of magnitude) can thus plausibly be associated with the point at which $\dot{M} \sim 0.3\dot{M}_{\text{edd}}$ (Steiner et al. 2009, 2010; Abramowicz et al. 2010). The jet luminosity and timescale of this transition also constrain the properties of the disrupted object and central BH (§4.2.3).

3.6 Stage 5: Jet Revival (Fig. 2e).

As \dot{M}_{fb} continues to decrease as a power-law in time, eventually it will reach a few percent of \dot{M}_{edd} . After this point the disk will again transition to a geometrically-thick disk, analogous to the ‘low/hard’ state observed in X-ray binaries. Since this state is conducive to jet formation (Narayan & Yi 1995; Fender et al. 2004), the jet in Sw J1644+57 and its associated X-ray emission may suddenly turn back on (this is estimated to occur sometime around 2016–2022; §5.5).

4 CONSTRAINTS ON Sw J1644+57

4.1 Stellar Progenitor Scenarios

We begin by overviewing the possible classes of stellar progenitors which could be responsible for Sw J1644+57. TD scenarios usually consider the disruption of a lower main sequence star. However, in principle the star could have been a giant (MacLeod et al. 2012), white dwarf (e.g. Krolik & Piran 2011; Haas et al. 2012; Shcherbakov et al. 2012), or even a planet. Low mass planets seem to be ruled out because the [beaming-corrected] energy budget of Sw J1644+57 of $\gtrsim \text{few} \times 10^{51}$ erg already exceeds the rest mass energy of Jupiter. A giant star is also unlikely, because the fall-back time of the stellar debris would greatly exceed the observed trigger time (§4.2.1), incompatible with the observed X-ray light curve. However, a white dwarf companion cannot be ruled out *a priori*, especially considering their potential for harboring a large magnetic flux.

In what follows, we thus consider constraints based on two progenitor scenarios: a lower main sequence star (MS) and a white dwarf (WD). We employ approximate mass-radius relations for each given by

$$\begin{aligned} r_{\star} &= m_{\star}, & [\text{MS}] \\ r_{\star} &= 0.013(m_{\star}/0.6)^{-1/3}, & [\text{WD}] \end{aligned} \quad (10)$$

where m_{\star} is in solar masses and r_{\star} is in solar radii. Since the stellar radius must exceed the tidal radius, only low mass black holes with

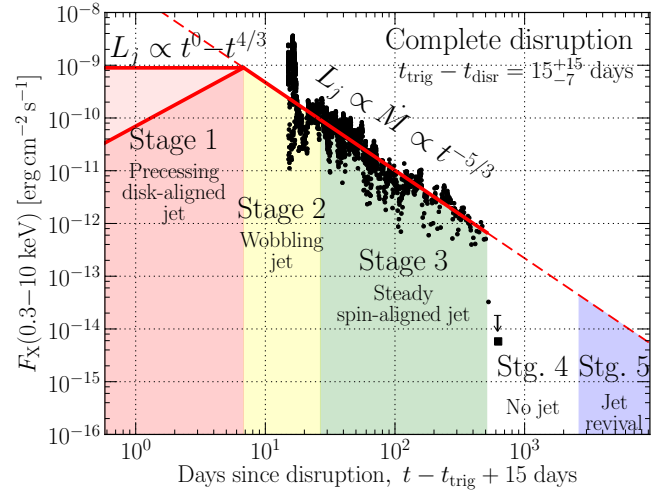


Figure 5. Sw J1644+57’s soft X-ray lightcurve accounting for the best-fit time of the disruption, $t_{\text{trig}} - t_{\text{disr}} = 15$ days before the trigger, for a *complete* disruption (see also Fig. 1). Note that just this simple shift in the zero point in time causes the early-time ‘plateau’ in the light curve (see Fig. 1) to disappear and the entire light curve to become consistent with a single power-law dependence in time, $\propto t^{-5/3}$. Various stages of the disruption process are indicated with color coding and text. These stages are explained in Fig. 2 and its caption.

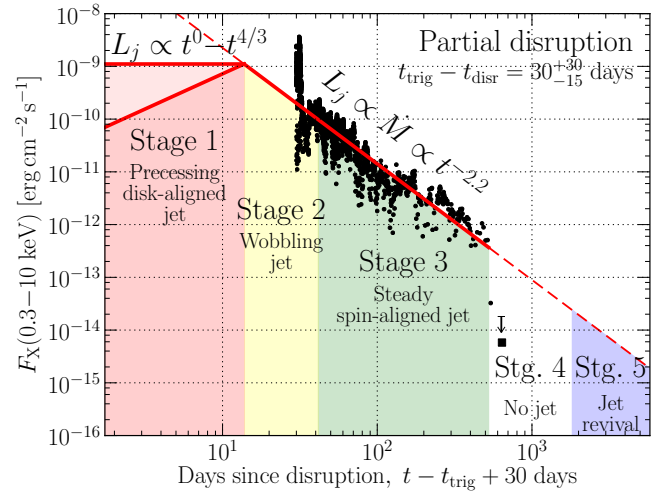


Figure 6. Sw J1644+57’s soft X-ray lightcurve accounting for the best-fit time of the disruption, $t_{\text{trig}} - t_{\text{disr}} = 30$ days before the trigger, for a *partial* disruption (see also Fig. 1). The steeper time-dependence of mass-fallback rate than in a complete disruption, $\propto t^{-2.2}$, allows for a longer delay between the time of the disruption and the time of the γ -ray trigger.

$M_{\bullet} \lesssim 10^5 - 10^6 M_{\odot}$ are capable of disrupting a WD, depending on WD mass and BH spin (Kesden 2012). For a centrally-concentrated MS star, the disruption process can be either ‘full’ or ‘partial’ (Guillochon & Ramirez-Ruiz 2012), resulting in different predictions for the rate of fall-back accretion (§4.2.1).

In what follows we thus consider three scenarios: (i) a complete or (ii) partial tidal disruption of a lower mass main-sequence star by a supermassive BH; or (iii) a complete disruption of a white dwarf by an intermediate-mass BH.

4.2 Observational Constraints

For each progenitor scenario our goal is to determine the following 4 unknowns: BH mass, $M_{\bullet,5}$, BH spin, a , stellar mass, m_{\star} , and magnetic flux threading the hole, Φ_{\bullet} . We now discuss what observational data constrain these properties within the framework of our model for Sw J1644+57.

4.2.1 Shape of the X-Ray Light Curve

First consider what constraints can be placed on Sw J1644+57 based on the shape of the X-ray light curve. Recall that although the time-averaged light curve does not follow a single power-law decay if plotted against the time since the γ -ray trigger $t - t_{\text{trig}}$, a much better fit is achieved by moving the TD ‘zero point’ prior to the trigger (Fig. 1). We thus first consider what range of trigger delay time $t_{\text{trig}} - t_{\text{disr}}$ produces a light curve shape consistent with the predicted power-law decline in the X-ray luminosity $L_X \propto \dot{M}_{\text{fb}} \propto (t - t_{\text{disr}})^{-\alpha}$ given the expected range in α .

Although the canonical value of $\alpha = 5/3$ is often quoted, α actually depends on the fraction of mass lost by the star during TD, $\Delta M_{\star}/M_{\star} = 0.4 f_{0.4}$, which differs between complete and partial disruptions (Guillochon & Ramirez-Ruiz 2012). If $\Delta M_{\star}/M_{\star} \approx 10\% - 50\%$ then $\alpha = 2.2$, but if $\Delta M_{\star}/M_{\star} \gtrsim 50\%$ then the value of α approaches that for a complete disruption, $\alpha = 5/3$ (Guillochon & Ramirez-Ruiz 2012). By considering the two limiting cases of complete disruptions with $\alpha = 5/3$ and partial disruptions with $\alpha = 2.2$, we bracket the allowed range of possibilities.

For complete disruptions ($\alpha = 5/3$) we find an allowed range of $t_{\text{trig}} - t_{\text{disr}} \sim 15_{-7}^{+15}$ days when fitting to the shape of the time-averaged X-ray light curve. Figure 5 shows the trigger delay-corrected light curve for a fiducial value $t_{\text{trig}} - t_{\text{disr}} = 15$ days. For partial disruptions ($\alpha = 2.2$), we find required delay times that are somewhat longer $t_{\text{trig}} - t_{\text{disr}} \sim 30_{-15}^{+30}$ days. Figure 6 shows the corrected light curve in this case for a fiducial delay $t_{\text{trig}} - t_{\text{disr}} = 30$ days.

Our fits quoted above (Figs. 5, 6) were made by matching the fall-back accretion rate \propto jet power to the time-averaged X-ray flux. However, if the early phase of high variability indeeds results from a ‘wobbling’ jet (§3.3), then bright flares may arise from transient episodes when the jets points towards our line of site. In this case, it is more physical to match the fall-back rate \propto jet power to the ‘envelope’ in the X-ray light curve comprised by the flare peaks, since these better characterize the true jet power. Since the observed duty cycle of the flaring state is $\sim 10\%$, this implies that the jet points towards us only about 1/10 of the time if the wobbling scenario is correct. The total jet power [accounting for both on- and off-axis jet emission] could thus exceed the observed [on-axis] emission by an order of magnitude (see also §5.4). Figure 1 shows that such fits allows for a trigger delay $t_{\text{trig}} - t_{\text{disr}}$ as short as a few days, consistent with the first evidence for a jet in Sw J1644+57 ~ 4 days prior to the γ -ray trigger (Krimm & Barthelmy 2011).

Given the allowed range in t_{trig} , we require that the fallback accretion rate must be past its peak at the trigger:

$$t_{\text{peak}} = 1.5 t_{\text{fb}} < t_{\text{trig}}/(1+z), \quad (11)$$

where the fall-back time (eq. [4]) specialized to WD and MS scenarios is given by

$$t_{\text{fb}} = 0.02 \text{ d } M_{\bullet,5}^{1/2} m_{\star}^{-3/2}, \quad [\text{WD}] \quad (12a)$$

$$t_{\text{fb}} = 17.3 \text{ d } M_{\bullet,5}^{1/2} m_{\star}^{1/2}, \quad [\text{MS}], \quad (12b)$$

since otherwise the light curve would still be rising and hence

would not match the $L_X \propto \dot{M}_{\text{fb}} \propto (t/t_{\text{fb}})^{-\alpha}$ decay predicted for $t \gg t_{\text{fb}}$.

4.2.2 Magnetic Flux

Although it does not represent an independent constraint, the magnetic flux Φ_{\bullet} is determined once the spin of the BH is known, if one assumes that the jet is in a MAD state after the trigger, up until the point when the jet shuts off. During MAD accretion, the BH magnetic flux is regulated by the mass accretion rate to a dimensionless value (Tchekhovskoy et al. 2012; Tchekhovskoy & McKinney 2012a), which is well approximated as

$$\text{In a MAD: } \phi_{\bullet}^{\text{MAD}} \equiv \frac{\Phi_{\bullet}^{\text{MAD}}}{(\dot{M}_g c)^{1/2}} \approx 70(1 - 0.38\omega_H)h_{0.3}^{1/2}, \quad (13)$$

corresponding to absolute flux

$$\text{In a MAD: } \Phi_{\bullet,30}^{\text{MAD}} = 0.067 M_{\bullet,5}^{3/2} \lambda^{1/2} (1 - 0.38\omega_H) h_{0.3}^{1/2}, \quad (14)$$

where $\lambda = \dot{M}/\dot{M}_{\text{Edd}}$ is the Eddington ratio and $h/r = 0.3h_{0.3}$ is the thickness of the accretion flow. Thus, if the dimensionless BH spin and the jet luminosity at a given Eddington ratio are known (such as at the point of jet shut-off; see eq. [15] below), then Φ_{\bullet} can be determined.

4.2.3 Jet Shut-Off Power

Another constraint is that the time at which the jet was observed to shut-off $t_{\text{off}} - t_{\text{trig}} \approx 500$ days (see Fig. 1) happens simultaneously with the expected state transition occurring at a fraction of the Eddington accretion rate (§2.5), i.e.

$$\dot{M}_{\text{cr}} = 0.3 \frac{\lambda_{\text{cr}}}{0.3} \dot{M}_{\text{Edd}}, \quad (15)$$

where theoretical and observational uncertainties place the threshold value in the range $0.1 \lesssim \lambda_{\text{cr}} \lesssim 0.5$.

Just prior to when the jet shut off, its X-ray luminosity \propto jet power P_j^{off} was ~ 200 times smaller than its value at the end of the ~ 10 day plateau phase after the trigger,

$$P_j^{\text{off}} \simeq (1/200) P_j^{\text{trig}} \approx 5 \times 10^{43} \frac{f_b \epsilon_{\text{bol}} \epsilon_X^{-1}}{0.03} \text{ erg s}^{-1}. \quad (16)$$

Now, by combining equations (3) and (13), the jet power can be written:

$$\begin{aligned} \text{In a MAD: } P_j &\approx F(\omega_H) h_{0.3} \dot{M} c^2 \approx 1.3 h_{0.3} a^2 \dot{M} c^2 \\ &\approx 1.6 \times 10^{44} h_{0.3} \lambda M_{\bullet,5} a^2 \text{ erg s}^{-1}, \end{aligned} \quad (17)$$

where $\lambda \equiv \dot{M}/\dot{M}_{\text{Edd}}$ and we used the fact that the spin-dependent factor entering jet power, $F(\omega_H) = 4.4\omega_H^2(1 - 0.38\omega_H)^2 f(\omega_H)$, can be approximated as $F \approx 1.3a^2$ to 10% accuracy for $0.3 \leq a \leq 1$ (Tchekhovskoy & McKinney 2012a).

Matching the jet power with the observed power (eq. [16]) at $\dot{M} = \dot{M}_{\text{cr}}$ (eq. [15]) thus requires

$$a^2 M_{\bullet,5} = \frac{f_b \epsilon_{\text{bol}} \epsilon_X^{-1}}{0.03} \frac{0.3}{\lambda_{\text{cr}}} \frac{0.3}{h/r}. \quad (18)$$

This constraint is independent of the nature of the disrupted object.

4.2.4 Jet Shut-Off Accretion Rate

Another constraint is that the BH mass accretion rate must equal the critical accretion rate (eq. [15]) at the observed jet shutoff time, $t_{\text{off}} - t_{\text{trig}} \simeq 500$ days, viz.

$$\dot{M}(t_{\text{off}}) = \dot{M}_{\text{cr}}, \quad (19)$$

where $\dot{M} = f_{\text{acc}} \dot{M}_{\text{fb}}$ and the predicted fall-back accretion rate (eqs. [4]–[6]) specialized to the MS and WD scenarios:

$$\dot{M}_{\text{fb}} = 4.2 \times 10^{28} M_{\bullet,5}^{1/3} m_{\star}^{4/3} t_1^{-5/3} \text{ g s}^{-1}, \quad [\text{MS, complete}] \quad (20)$$

$$\dot{M}_{\text{fb}} = 1.2 \times 10^{29} f_{0.4} M_{\bullet,5}^{3/5} m_{\star}^{8/5} t_1^{-2.2} \text{ g s}^{-1}, \quad [\text{MS, partial}] \quad (21)$$

$$\dot{M}_{\text{fb}} = 4.6 \times 10^{26} M_{\bullet,5}^{1/3} t_1^{-5/3} \text{ g s}^{-1}, \quad [\text{WD, complete}] \quad (22)$$

where $t_1 \equiv t/\text{day}$.

The factor $f_{\text{acc}} < 1$ accounts for the possibility that only a fraction of the fall-back material actually reaches the BH horizon, with the rest either expelled in the form of the accretion disk winds and or lost during the circularization of the tidal streams. Super-Eddington accretion is susceptible to outflows driven by radiation pressure (e.g. Ohsuga et al. 2005, Strubbe & Quataert 2009), but the magnitude of this effect is uncertain. Fortunately, we find that the lower limit on f_{acc} is not constraining (§4.3), so without the loss of generality we allow the full range $0 < f_{\text{acc}} \leq 1$ in our calculations.

4.2.5 Spin Sufficient for Alignment

We require that the spin of the BH to be sufficiently high,

$$a \gtrsim 0.5, \quad (23)$$

such that the BH is able to magnetically align the disk and the jets (MTB12a).

4.2.6 MAD QPO

A final possible constraint is to match the QPO period measured in the power-law X-ray light curve of Sw J1644+57 (Reis et al. 2012)

$$\tau_{\text{QPO}} = 210 \pm 30 \text{ s}. \quad (24)$$

with the predicted MAD QPO, which occurs at a frequency that is 1/4 of BH horizon angular frequency (McKinney et al. 2012b), $\Omega_{\text{H}} = ac/(2r_{\text{H}}) = \omega_{\text{H}}c/(2r_{\text{g}})$, resulting in a predicted period

$$\tau_{\text{MAD}} = \frac{2\pi}{0.25\Omega_{\text{H}}} = \frac{16\pi r_{\text{g}}}{\omega_{\text{H}} c} = 24.8 M_{\bullet,5} \omega_{\text{H}}^{-1} \text{ s}. \quad (25)$$

Equating (25), multiplied by $(1+z) \approx 1.353$, with (24) gives a final constraint,

$$M_{\bullet,5} = (6.3 \pm 0.9)\omega_{\text{H}}. \quad (26)$$

We show below that this requirement is constraining only in the WD scenario.

4.3 Results

Equations (11), (18), (19), (23) and (26) provide 4 or 5 constraints on the unknown parameter space (M_{\star} , M_{\bullet} , a), depending on whether one adopts the (speculative) QPO constraint described in §4.2.6. Once M_{\bullet} and a are determined, the magnetic flux Φ_{\bullet} follows from equation (14). We now apply these constraints individually to each of our proposed scenarios (§4.1): Complete Disruption

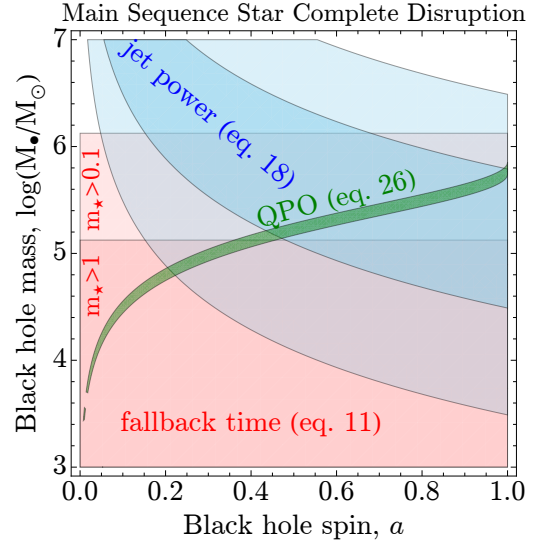


Figure 7. Constraints on BH mass, M_{\bullet} , and spin, a , in the scenario of a complete disruption of a lower-mass main-sequence star. The constraint on jet power at jet shut off [eq. (18)] gives the blue-shaded regions, with the darker shaded region more likely. The constraint on disruption timescale [eq. (11)] gives the dark (light) shaded red regions for $m_{\star} > 1$ ($m_{\star} > 0.1$, respectively). The QPO period constraint [eq. (26)] gives the green curve. The common region seems to favor a lower-mass star, $m_{\star} \sim \text{few} \times 0.1$, and a light BH, $M_{\bullet,5} \sim \text{few}$, with $a \gtrsim 0.5$.

of a Main Sequence Star (§4.3.1); Partial Disruption of a Main Sequence Star (§4.3.2); and Complete Disruption of a White Dwarf (§4.3.3).

4.3.1 Complete Disruption of a Main-Sequence Star

Figure 7 summarizes the constraints on the BH mass and spin for the complete tidal disruption of a low mass MS star. The first constraint, based on the shape of the X-ray light curve (eq. [11]), can be written

$$M_{\bullet,5} < 1.3 m_{\star}^{-1}, \quad (27)$$

where we have adopted the highest value for $t_{\text{trig}} = 30$ days that allows us to reproduce the observed shape of the X-ray lightcurve (Figs. 1, 5). This constraint is shown in Figure 7 as the dark (light) red shaded regions for $m_{\star} \geq 1$ ($m_{\star} \geq 0.1$).

For a solar mass star, equation (27) places a tight upper limit on the BH mass, $M_{\bullet} < 1.3 \times 10^5 M_{\odot}$. Such a low mass BH would be novel since they are quite rare (either intrinsically, or due to the observational challenges in detecting them; e.g. Greene 2012) and might be unexpected given the host galaxy of Sw J1644+57. A higher mass $M_{\bullet} \gtrsim \text{few} \times 10^5 M_{\odot}$ is allowed if the mass of the star is lower, $m_{\star} \lesssim 0.5$, below the peak of the standard IMF (Chabrier 2003).

The second constraint (eq. [18]) cuts out a stripe in the M_{\bullet} – a plane, as shown as a blue-colored region in Figure 7. The width of the dark (light) blue region reflect an optimistic (conservative) factor of 20 (1000) uncertainty in the value of the right-hand side of equation (18). The chief effect of this constraint is to place a lower limit on the BH mass and spin, the latter consistent with the fourth constraint (§4.2.5).

The third constraint (eq. [19]) does not place an interesting limits on BH mass or spin due to the uncertainty in the fraction

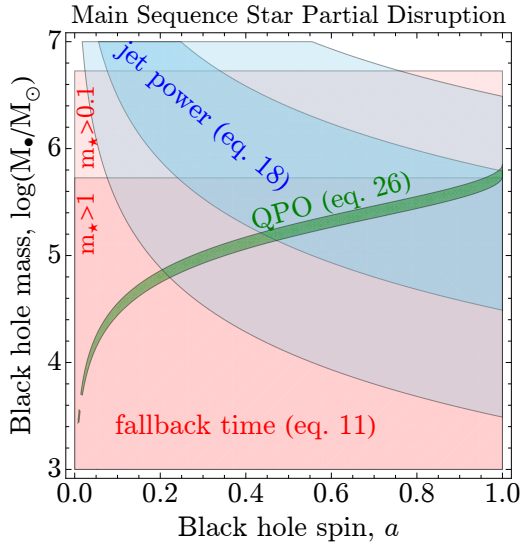


Figure 8. Constraints on BH mass, M_* , and spin, a , in the scenario of a partial disruption of a lower-mass main-sequence star. The constraint on jet power at jet shut off [eq. (18)] gives the blue-shaded regions, with the darker shaded region more likely. The constraint on disruption timescale [eq. (11)] gives the dark (light) shaded red regions for $m_* > 1$ ($m_* > 0.1$, respectively). The QPO period constraint [eq. (26)] gives the green curve. The common region (including the QPO constraint) allows a Sun-like star, $m_* \lesssim 1$, and a super-massive BH, $M_{*,5} \lesssim 5$, with $a \gtrsim 0.5$.

of the stellar material accreted f_{acc} . However, it does pick out a preferred range in the value of f_{acc} given the other parameters:

$$f_{\text{acc}} = 0.02 \frac{\lambda_{\text{cr}}}{0.3} M_{*,5}^{2/3} m_*^{-4/3} < 0.024 \frac{\lambda_{\text{cr}}}{0.3} m_*^{-2}, \quad (28)$$

where in the inequality we have used equation (27). Equation (28) shows that if the tidally disrupted star was solar-like ($m_* \sim 1$), then large mass loss is required, as could be the result of outflows from the disk or at the impact point of tidal streams. Alternatively, a higher value $f_{\text{acc}} \sim 1$ is allowed if the progenitor is instead a low mass M star $m_* \sim 0.1 - 0.2 M_\odot$ near the hydrogen-burning limit.

The fifth constraint, on the QPO frequency, produces an allowed region shown with green in Fig. 7, which is consistent with (and does not appreciably alter) our conclusions above. If taken seriously, this constraint places an upper limit on the BH mass $M_* < 6 \times 10^5 M_\odot$, but otherwise a wide range of BH spin, $a \gtrsim 0.5$, is allowed.

4.3.2 Partial Disruption of a Main-sequence Star

Figure 8 summarizes the constraints on the BH mass and spin based on our second scenario, the partial tidal disruption of a lower-mass MS star. As in equation (27), the first constraint can be written

$$M_{*,5} < 5.3 m_*^{-1}, \quad (29)$$

where here we have taken $t_{\text{trig}} = 60$ days (again as the maximum allowed by fitting the observed shape of the light curve; §4.3.1). Constraint (29) is a factor of several less restrictive than that for a complete disruption (eq. 27). For example, the data now allow a relatively massive BH with $M_* \gtrsim \text{few} \times 10^5 M_\odot$, even for a Sun-like star, $m_* \simeq 1$.

The region allowed by the second constraint (eq. [18]; again shown in blue) is exactly the same as for the full disruption (Fig. 7).

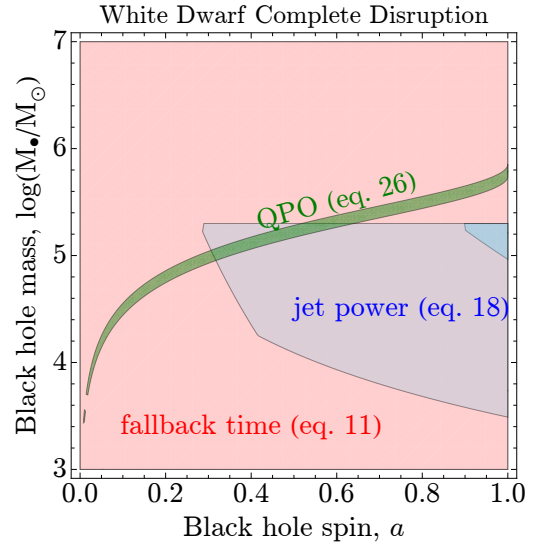


Figure 9. Constraints on BH mass, M_* , and spin, a , in the scenario of a complete disruption of a white dwarf. The constraint on jet power at jet shut off [eq. (18)] gives the blue-shaded regions, with the darker shaded region more likely. This darker shaded region appears marginally within the bounds of this plot and requires extreme BH spin: this is due to limited mass supply of the WD that has hard time to power the jets as strong as they are observed. The constraint on disruption timescale [eq. (11)] allows all of the parameter space. We conclude that WD disruption scenario is possible for intermediate mass BHs, with $M_{*,5} = 0.1-2$ and $a \gtrsim 0.5$. In addition to requiring an intermediate-mass BH, the WD scenario also requires very small jet opening angles and small bolometric correction, $f_{\text{bol}} < 5 \times 10^{-4}$. Thus, we suggest that the WD disruption scenario is less likely than a MS star disruption. Accounting for the QPO period constraint [eq. (26)], which is shown with the green curve, constrains the BH spin to $a \sim 0.5$.

The QPO condition is again only moderately constraining, placing an upper limit $M_{*,5} < 6 \times 10^5 M_\odot$ on the BH mass.

Similar to the full disruption, the third constraint does not place any interesting limits on the BH or stellar parameters, but it does tell us the fraction,

$$f_{\text{acc}} = 0.2 f_{0.4} \frac{\lambda_{\text{cr}}}{0.3} M_{*,5}^{2/5} m_*^{-8/5} < 0.39 f_{0.4} \frac{\lambda_{\text{cr}}}{0.3} m_*^{-2}. \quad (30)$$

of the fallback material reaching the BH, where equation (29) is used in the last inequality. For low mass stars the required value of f_{acc} may even exceed unity, potentially ruling out such progenitors depending on the value of $\lambda_{\text{cr}} \sim 0.1 - 0.5$. This behavior is opposite to that in the complete MS disruption scenario, where we were forced to conclude that $f_{\text{acc}} \ll 1$ [eq. (28)]. As we discussed in §4.2.1, the two extreme possibilities—of a complete and partial disruption—bracket a continuous family of allowed solutions that, by continuity, are consistent with the data.

4.3.3 Complete Disruption of a White Dwarf

Figure 9 summarizes the constraints on the BH properties based on our third scenario, the disruption of a WD. Since a WD is much denser than a MS star, the fallback time in the WD scenario is much shorter than in the MS scenario. In fact, $t_{\text{fb}} \ll t_{\text{trig}}$, where $t_{\text{trig}} \gtrsim 5$ days is required to explain the shape of the X-ray lightcurve to within a factor of few (see §4.2.1). For these reasons, the first constraint, (11), does not place interesting limits on the system parameters.

The most important constraint is that on the accretion rate, eq. (19), which gives

$$f_{\text{acc}} = 2 \frac{\lambda_{\text{cr}}}{0.3} M_{\bullet,5}^{2/3}. \quad (31)$$

The physical requirement that $f_{\text{acc}} < 1$ places an upper limit on the BH mass, $M_{\bullet,5} \lesssim 2$ (for $\lambda_{\text{cr}} > 0.1$), thus *requiring an intermediate-mass BH*.

Since the mass fallback rate is independent of the WD mass (eq. [22]), this makes the second constraint, eq. (18), on jet power particularly constraining on the BH spin,

$$a = 1.6 \left(\frac{f_{\text{b}} \epsilon_{\text{bol}} \epsilon_X^{-1}}{0.03} \right)^{1/2} \left(\frac{\lambda_{\text{cr}}}{0.3} \right)^{1/4} f_{\text{acc}}^{-3/4} h_{0.3}^{-1/2}. \quad (32)$$

The constraints resulting from eqs. (31) and (32) are illustrated in Figure 9 with the dark (light) blue area, whose width reflects optimistic (conservative) modeling and observational uncertainties of a factor 20 (100) in the right-hand side of eq. (18). The most likely (dark blue region) favors a high BH spin, $a \gtrsim 0.9$.

The addition of the less certain QPO constraint (eq. 26) in combination with the spin constrain (eq. 23) favors a BH mass in the range $M_{\bullet,5} \sim 0.6 - 2$ with an intermediate spin $a \approx 0.5$. However, we caution against over-interpreting the QPO constraint, as the observed QPO could be caused by other processes than those resulting from MAD accretion (McKinney et al. 2012b).

Finally, we note that *partial* disruption of a WD is less plausible than a complete disruption due to the lower mass fall-back rate and the steeper time-dependence of \dot{M}_{fb} (eq. [22]). This makes constraint (32) much more severe, causing tension with the observations. For this reason, we focus exclusively on complete disruption in the WD case.

5 DISCUSSION

5.1 Nature of the Disrupted Star

In §4.1 we introduced three plausible scenarios for the nature of the disrupted object: a MS star (full or partial disruption) and a WD (full disruption). We find that a MS stellar disruption comfortably satisfies all of the observational constraints (§4.2; Figs. 7, 8) for a BH with mass $M_{\bullet} \sim (\text{few} - 10) \times 10^5 M_{\odot}$ which is consistent with upper limits based on X-ray variability and the host galaxy of Sw J1644+57 (Levan et al. 2011; Bloom et al. 2011; Burrows et al. 2011). Both complete and partial disruption are allowed. A complete disruption favors lower-mass stars, $M_{\star} \lesssim 0.5 M_{\odot}$, while a partial disruption (in which a star loses 10 to 50% of its mass while its core survives) allows a wide range of stellar masses, $M_{\star} = (0.1 - 1) M_{\odot}$. Complete disruptions of more massive stars ($M_{\star} \sim M_{\odot}$) are also allowed but require (potentially rare) smaller-mass BHs ($M_{\bullet} \lesssim 10^5 M_{\odot}$).

Unlike a MS star disruption, WD disruptions require the central object to be an intermediate-mass BH of mass $M_{\bullet} = (1 - 10) \times 10^4 M_{\odot}$ (§4.3.3; Fig. 9). In addition, the mass fallback rate in the WD case is just barely sufficient to power the observed jets, which thus greatly restricts the allowed parameter space (§4.3.3).

Although the WD scenario is formally allowed, there are several reasons to favor the MS scenario. In addition to the narrow allowed parameter space in the WD case, the probability of WD disruption is much lower than in the MS since its smaller tidal radius limits the allowed range of impact parameters capable of resulting in disruption. Furthermore, the intermediate-mass BH required in the WD case is an exotic, and probably rare, object (Greene

2012); it is also unclear how frequently such an object would be expected to reside near the nucleus of a galaxy. Given the convergence of several rare events in the WD scenario, we conclude that a MS disruption is more likely. The existence of plausible and constrained solutions provides a consistency check on our model for Sw J1644+57.

In addition to jetted emission, TD events are accompanied by thermal optical/UV/soft X-ray emission from the accretion disk (e.g. Ulmer 1999) or super-Eddington outflows (Strubbe & Quataert 2009, 2011). No such optical/UV emission was detected from Sw J1644+57, possibly due to substantial dust extinction (Bloom et al. 2011). However, if an otherwise similar event with less extinction were to occur in the future, a measurement of the disk flux just after the jet shuts off would directly determine λ_{cr} , the critical Eddington ratio at which the disk transitions from being thick to thin. Combined with the jet-related constraints in §4.2, such a measurement would also better determine the properties of the BH and disrupted star.

5.2 Origin of the Magnetic Flux

Regardless of the nature of the disrupted star, the magnetic flux threading the BH must be sufficient to power jet responsible for Sw J1644+57. Equation (2) can be written as:

$$\Phi_{\bullet,30}^{\text{trig}} \approx 0.4 M_{\bullet,5} \left(\frac{P_{\text{j}}^{\text{trig}}}{10^{46} \text{ erg s}^{-1}} \right)^{1/2} \left(\frac{\omega_{\text{H}} f^{1/2}(\omega_{\text{H}})}{0.64} \right)^{-1} \quad (33)$$

where $\omega_{\text{H}} f^{1/2}(\omega_{\text{H}})$ is normalized to its value for BH spin $a = 0.9$. If the onset of MAD indeed occurred near the time of the γ -ray trigger (at Eddington ratio $\lambda_{\text{trig}} \approx 200 \lambda_{\text{cr}} \approx 60(\lambda_{\text{cr}}/0.3)$; see §4.2.3), then we require $\Phi_{\bullet,30}^{\text{MAD}} \sim 0.1 - 10$ for BH masses $M_{\bullet,5} \sim 0.1 - 10$ consistent with our modeling of Sw J1644+57 (Figs. 7-9). This flux is $\sim 4 - 6$ orders of magnitude greater than that through a solar-type star $\Phi_{\star} \sim \pi B_{\star} R_{\star}^2 = 10^{25} (B_{\star}/\text{kG})(R_{\star}/R_{\odot})^2 \text{ G cm}^2$, even for an optimistically large $B_{\star} \sim \text{kG}$ average stellar magnetic field. Likewise, a WD ($R_{\star} \sim 0.01 R_{\odot}$) would require a field $B_{\star} \gtrsim 10^{11} \text{ G}$ for $M_{\bullet,5} \sim 1$ (Fig. 9) which exceeds the largest measured [surface] fields by two orders of magnitude (e.g. Kepler et al. 2012).

If the star itself cannot explain the flux, what could be its source? It has been suggested (Krolik & Piran 2011, 2012) that the requisite flux is generated by a turbulent dynamo in the accretion flow. However, since the *net* vertical magnetic flux is a conserved quantity in ideal MHD, then the vertical component of the field must undergo a random walk about zero (if not, then what determines a preferred direction?), such that the BH periodically receives patches of random polarity. The characteristic timescale between such flips in the mean field would presumably be set by the accretion timescale near the outer radius of the disk R_{circ} , which is $t_{\text{visc}} \sim 10^3 \text{ s}$ and $\sim 10^6 \text{ s}$ in the case of WD and MS stars, respectively (see §5.3). Without a large-scale magnetic flux to produce a sustained jet, such polarity flips would cause the jet power to transiently switch off each time the flux changes sign (Beckwith et al. 2008; McKinney & Blandford 2009; McKinney et al. 2012b) at characteristic intervals $\sim t_{\text{visc}}$. Such large-scale variability is not obviously seen in Sw J1644+57 lightcurve after the first ~ 10 days, once it has settled into a magnetically-arrested state. Instead, the fact that Sw J1644+57 was continuously active over nearly 1.5 years may suggest that the BH must be threaded by large-scale magnetic flux of the same sign. Although it is difficult to rule out a dynamo process completely, since the physics of large-scale magnetic field generation in accretion disks is at best poorly

understood, we instead focus on the possibility that a reservoir of large-scale magnetic flux is required.

A possible source of large-scale flux is that contained in a pre-existing (‘fossil’) accretion disk, which was present at the time of TD but was not detectable in pre-imaging of the host of Sw J1644+57 since its accretion rate was relatively low (Eddington ratio $\lambda_{\text{fossil}} \lesssim 10^{-2}$). During the disruption process, stellar debris is flung outwards onto a series of highly eccentric orbits with an apocenter radius (e.g. Strubbe & Quataert 2009)

$$\frac{r_a}{r_g} \approx 2 \left(\frac{ct}{2\pi r_g} \right)^{2/3} \approx 1.3 \times 10^4 M_{\bullet,5}^{-1/3} m_{\star}^{-2/3} r_{\star} \left(\frac{t}{t_{\text{fb}}} \right)^{2/3}. \quad (34)$$

that increases for material with fall-back times longer than that of the most bound stellar debris t_{fb} , where the prefactor in equation (34) is calculated for a solar mass star. Thus, as debris returns to the BH, it sweeps up a significant fraction⁵ of the magnetic flux threading the fossil disk at radii $r < r_a(t)$.

We now estimate how luminous the jet from such a fossil disk would have to be in order to supply the required flux, assuming that the fossil disk is itself in a MAD state. In a MAD with a vertical thickness $h/r \approx 0.3$ – 0.6 (as characterizes both super-Eddington and highly sub-Eddington accretion), every $\Delta r \sim 30h_{0.3}r_g$ of the accretion disk contains as much magnetic flux as the BH itself (Tchekhovskoy & McKinney 2012b; McKinney et al. 2012a), where $h/r = 0.3h_{0.3}$. Thus, the magnetic flux contained by a magnetically-arrested fossil disk out to a distance r is given by (Tchekhovskoy & McKinney 2012b; McKinney et al. 2012b),

$$\Phi_{\text{D}}^{\text{fossil}}(r) \approx \frac{r}{30r_g} \left(\frac{\lambda_{\text{fossil}}}{\lambda_{\text{MAD}}} \right)^{1/2} h_{0.3}^{-1} \Phi_{\bullet}^{\text{MAD}}, \quad (35)$$

where we used eq. (14) to relate the flux threading the BH by the quiescent disk to that in the MAD state of Sw J1644+57, viz. $\Phi_{\bullet}^{\text{fossil}} = (\lambda_{\text{fossil}}/\lambda_{\text{MAD}})^{1/2} \Phi_{\bullet}^{\text{MAD}}$. Since the apocenter distance of the infalling debris increases as $r_a \propto t^{2/3}$ (eq. 34), the cumulative amount of “fallback” magnetic flux, which is brought to the BH by the infalling tidal streams, is given by

$$\Phi_{30}^{\text{fb}}(t) \approx 0.43 \left(\frac{\lambda_{\text{fossil}}/\lambda_{\text{MAD}}}{10^{-6}} \right)^{1/2} \Phi_{\bullet,30}^{\text{MAD}} M_{\bullet,5}^{-1/3} m_{\star}^{-2/3} r_{\star} h_{0.3}^{-1} \left(\frac{t}{t_{\text{fb}}} \right)^{2/3} \quad (36)$$

$$\approx 0.38 \left(\frac{\lambda_{\text{fossil}}/\lambda_{\text{MAD}}}{10^{-6}} \right)^{1/2} M_{\bullet,5}^{2/3} m_{\star}^{-2/3} r_{\star} \times \left(\frac{P_j}{10^{46} \text{ erg s}^{-1}} \right)^{1/2} h_{0.3}^{-1} \left(\frac{t}{t_{\text{fb}}} \right)^{2/3}, \quad (37)$$

where in the last line we have used equation (33) and have assumed $a = 0.9$. Figures 3 and 4 show the time-evolution of Φ^{fb} in fiducial MS partial disruption and WD scenarios, respectively.

By demanding in equation (36) that at $t = t_{\text{peak}} \approx 1.5t_{\text{fb}}$ the accreted flux Φ_{fb} equal $\Phi_{\bullet}^{\text{MAD}}$, i.e. sufficient to magnetically-arrest the disk at $t = t_{\text{MAD}}$, this places a lower limit on the Eddington ratio of the fossil disk (using $\lambda_{\text{MAD}} \approx 60$):

$$\lambda_{\text{fossil}} > 2 \times 10^{-4} M_{\bullet,5}^{2/3} m_{\star}^{4/3} r_{\star}^{-2} (t_{\text{peak}}/t_{\text{MAD}})^{4/3}, \quad (38)$$

corresponding to a jet power of the fossil disk given by (eq. 17)

$$P_j^{\text{fossil}} \gtrsim 3 \times 10^{40} M_{\bullet,5}^{2/3} m_{\star}^{4/3} r_{\star}^{-2} (t_{\text{peak}}/t_{\text{MAD}})^{4/3} \text{ erg s}^{-1}. \quad (39)$$

⁵ Although the tidal debris traverses only a small fraction of the azimuthal extent of the disk, the time it spends at pericenter is comparable to the local orbital time. Thus, a large fraction of the disk will have sufficient time to rotate into, and be collected by, the debris before it falls back.

If we adopt bolometric and beaming corrections similar to that applied in Sw J1644+57, then the resulting X-ray luminosity $L_{\text{X,obs}} \gtrsim 5 \times 10^{41} M_{\bullet,5}^{2/3} m_{\star}^{4/3} r_{\star}^{-2} \text{ erg s}^{-1}$ to $t_{\text{MAD}} \sim t_{\text{peak}}$ is comfortably consistent with ROSAT upper limits $L_{\text{X}} \lesssim 2 \times 10^{44} \text{ erg s}^{-1}$ on prior activity from the host galaxy of Sw J1644+57 (Bloom et al. 2011) for $1 \lesssim M_{\bullet,5} \lesssim 10$.⁶ Thus, a fossil disk sufficiently dim to go undetected prior to Sw J1644+57 nevertheless could supply sufficient magnetic flux to power the observed jet.

5.3 Nature and Duration of the Flaring State

In our model for Sw J1644+57, the jets initially point along the rotation axis of the accretion disk, which is misaligned relative to the BH spin and our line of site (Stage 1 in Fig. 2). As \dot{M} decreases, however, magnetic flux accumulated on the BH becomes increasingly dynamically important and the disk enters a magnetically-arrested state, MAD (Narayan et al. 2003; Tchekhovskoy et al. 2011). Once in a MAD state, strong magnetic fields cause the inner disk and jet to align with the BH spin axis (Stage 2). However, this alignment process is erratic, with the jets periodically ramming against the accretion flow (MTB12a). Occasionally a strong flare is produced when the jet transiently aligns with our line of site, but at most times we observe emission originating from large angles off the core of the jet. This violent transition to a fully-aligned jet accounts for the extreme variability observed in Sw J1644+57 over the first 10 days after the γ -ray trigger (Bloom et al. 2011). Since the first evidence for a jet ~ 4 days prior to the trigger (Krimm & Barthelmy 2011; Burrows et al. 2011), the total duration of this flaring phase was at least two weeks.

Because the jet alignment is controlled by the magnetic field of the BH, the characteristic interval between flares is set by the timescale for magnetic flux accumulation. Recent simulations show that large fluctuations in the jet power (“flares”) are produced in MAD flows due to periodic accumulation and expulsion of flux by the BH on semi-regular intervals of $(0.5\text{--}2)10^3 M_{\bullet,5}$ seconds (Tchekhovskoy et al. 2011; Tchekhovskoy & McKinney 2012b). To understand this result, note that the inner $\sim 30h_{0.3}r_g$ of a MAD accretion disk contain as much flux as the BH itself (Tchekhovskoy & McKinney 2012b; McKinney et al. 2012b). Therefore, when the BH expels an order-unity fraction of its flux, this flux is replenished on a characteristic timescale set by the accretion time at $r \approx 15h_{0.3}r_g$,

$$\Delta t_{\text{flare}} \sim t_{\text{acc}} = \alpha_{\text{ss}}^{-1} \left(\frac{h}{r} \right)^{-2} \Omega_{\text{K}}^{-1} \approx 3 \times 10^3 \text{ s} \left(\frac{\alpha_{\text{ss}}}{0.1} \right)^{-1} h_{0.3}^{-1/2} M_{\bullet,5} \left(\frac{r}{15r_g} \right)^{3/2}, \quad (40)$$

where α_{ss} parameterizes the disk viscosity and $\Omega_{\text{K}} = (GM_{\bullet}/r^3)^{1/2}$ is the Keplerian orbital velocity. Equation (40) shows that Δt_{flare} is consistent with the observed interval $\text{few} \times 10^4$ seconds between the large-amplitude flares in Sw J1644+57 if the BH is moderately massive, $M_{\bullet,5} \gtrsim \text{few}$ (depending on α_{ss}).

In contrast to the interval between flares, the *total* duration of the flaring state must be at least as long as the accretion time scale

⁶ That said, it is not at all clear whether the jet from the fossil disk would indeed be pointed along our line of site (= spin axis of the BH) since although the disk is in a MAD state at small radii, the jet direction could be set by the plane of the disk on larger scales, where it is not magnetically-arrested and in general is misaligned with our line of site.

of the *entire* disk near its outer radius \sim the circularization radius. Substituting R_{circ} (eq. [8]) into equation (40), we find a flaring duration

$$\tau_{\text{acc}} \equiv t_{\text{acc}}(r = R_t) \approx 5 \times 10^5 \text{ s} \left(\frac{\alpha_{\text{ss}}}{0.1} \right)^{-1} h_{0.3}^{-1/2} m_* \beta^{-3/2} \quad [\text{MS}] \quad (41)$$

$$\approx 10^3 \text{ s} \left(\frac{\alpha_{\text{ss}}}{0.1} \right)^{-1} h_{0.3}^{-1/2} (m_*/0.6)^{-1} \beta^{-3/2}. \quad [\text{WD}] \quad (42)$$

Again, τ_{acc} is consistent with the duration of the flaring state in Sw J1644+57 ($\sim 10^6$ s) for a solar-type star with impact parameter $\beta \sim 1$, independent of the BH mass. However, for a WD τ_{acc} appears to be too short.

Although τ_{acc} [eq. (42)] sets the minimum duration of the flaring state, the state can last longer if the BH requires more time to fully align the accretion disk with the BH spin. Alignment completes only once the entire disk is magnetically-arrested. At the onset of a MAD, most of the [large-scale] magnetic flux in the system is concentrated near the BH. As time goes on, two processes take place. Firstly, the mass accretion rate drops, causing the centrally-concentrated magnetic flux to be redistributed to the outer regions of the accretion disk. Secondly, new flux is added at the outer edge of the disk by the infalling stellar debris that has picked up magnetic flux from the fossil accretion flow (§5.2). Since in a MAD every $\sim 30h_{0.3}r_g$ in radius holds roughly the same amount magnetic flux as the BH itself (Tchekhovskoy & McKinney 2012b), the whole disk goes MAD once its flux reaches a value

$$\Phi_{\text{D}}^{\text{max}} \approx \frac{R_{\text{circ}}}{30r_g} h_{0.3}^{-1} \Phi_{\bullet} \approx 15r_* m_*^{-1/3} M_{\bullet,5}^{-2/3} \beta^{-1} h_{0.3}^{-1} \Phi_{\bullet}, \quad (43)$$

where Φ_{D} is the total flux through the midplane of the disk and the last equality makes use of equation (8).

Now, the flux through the BH evolves as (see eq. 14):

$$\Phi_{\bullet} = \Phi_{\bullet}^{\text{MAD}} (t/t_{\text{MAD}})^{-\alpha/2}, \quad (44)$$

where $\Phi_{\bullet}^{\text{MAD}}$ is BH magnetic flux and t_{MAD} is the time at the onset of MAD near the hole. The fallback magnetic flux, brought in by the infalling debris, evolves as (see eq. 37):

$$\Phi^{\text{fb}} = \Phi_{\bullet}^{\text{MAD}} \left(\frac{t}{t_{\text{MAD}}} \right)^{2/3}. \quad (45)$$

The flux through the disk evolves as

$$\Phi_{\text{D}} = (\Phi_{\bullet}^{\text{MAD}} - \Phi_{\bullet}) + (\Phi^{\text{fb}} - \Phi_{\bullet}^{\text{MAD}}), \quad (46)$$

where the disk flux increases as the result of both flux leaving the BH (first term in parentheses) and new flux brought in by the infalling debris (second term in parentheses).

Condition (43) can now be written:

$$\begin{aligned} \frac{\tau_{\text{align}}}{t_{\text{MAD}}} &\approx \left(1 + \frac{\Phi_{\text{D}}^{\text{max}}}{\Phi_{\bullet}} \right)^{\gamma} \approx \left(1 + 15r_* m_*^{-1/3} M_{\bullet,5}^{-2/3} \beta^{-1} h_{0.3}^{-1} \right)^{\gamma} \quad (47) \\ &\approx \left[1 + 0.8 \left(\frac{m_*}{0.5} \right)^{2/3} \left(\frac{M_{\bullet,5}}{3} \right)^{-2/3} \left(\frac{\beta}{2} \right)^{-1} \left(\frac{h_{0.3}}{3} \right)^{-1} \right]^{2/3}, \quad [\text{MS, complete}] \quad (48) \end{aligned}$$

$$\approx \left[1 + 1.9 \left(\frac{m_*}{0.5} \right)^{2/3} \left(\frac{M_{\bullet,5}}{3} \right)^{-2/3} \left(\frac{\beta}{0.8} \right)^{-1} \left(\frac{h_{0.3}}{3} \right)^{-1} \right]^{0.57}, \quad [\text{MS, partial}] \quad (49)$$

$$\approx \left[1 + 0.4 \left(\frac{m_*}{0.6} \right)^{-2/3} \left(\frac{M_{\bullet,5}}{0.1} \right)^{-2/3} \beta^{-1} \left(\frac{h_{0.3}}{3} \right)^{-1} \right]^{2/3}, \quad [\text{WD, complete}] \quad (50)$$

where $\gamma = 6/(4 + 3\alpha)$, and the last three lines are evaluated for our three progenitor scenarios (§4.1). Equation (47) shows that the jet alignment (flaring) phase can last for a timescale comparable (or somewhat longer than) than that required for the MAD to form. For a MS star, both τ_{acc} [eq. (42)] and τ_{align} [eq. (47)] are sufficiently long to account for the observed duration of the flaring state in Sw J1644+57. However, for a WD, although τ_{acc} is very short, the duration of the flaring state is set by $\tau_{\text{align}} \sim t_{\text{MAD}}$ and hence (since $t_{\text{MAD}} \sim t_{\text{trig}} \sim$ days) is also consistent with observations.

Many of the points above are illustrated explicitly in Figures 3 and 4, which shows the time-evolution of Φ_{D} and Φ_{\bullet} in fiducial MS partial disruption and WD scenarios, respectively. In both cases, Φ_{\bullet} initially rises with the accumulated flux Φ_{fb} , until the inner disk near the BH becomes magnetically arrested. After this point, flux leaks out of the BH into the surrounding disk and new flux is added by fallback material at the outer edge of the disk (Φ_{D} rises). However, eventually \dot{M} drops sufficiently for the entire disk to become magnetically arrested (magnetic field marginally dynamically-important everywhere). At this point, even the disk itself cannot hold the accumulated flux, which begins to leak out, causing Φ_{D} to fall. The jet alignment/flaring phase described above (Stage 2) occurs during the interval when Φ_{D} is still rising.

5.4 Origin of Radio Rebrightening

Our fits to the X-ray light curve of Sw J1644+57 (Figs. 1, 5, 6) show that the jet could have been active weeks-month prior to the first detection. However, since the jet was pointed away from—and possibly precessing about—our line of site (= spin axis of the BH), its emission was not initially observable due to geometric or relativistic beaming. Nevertheless, since the jet still injects relativistic kinetic energy into the surrounding ISM during this phase, this gives rise to delayed radio afterglow emission on a timescale of months–year for a typical misalignment angle (§2.3), consistent with observed radio re-brightening several months after the trigger (B12).

To produce radio rebrightening of the magnitude observed in Sw J1644+57, the additional energy released by the early off-axis jet must exceed that released later during the on-axis phase (i.e. after the initial γ -ray detection). Since the mass accretion rate decreases as $\dot{M} \propto t^{-\alpha}$ and the jet power $P_j \propto \dot{M}$ [eq. (17)] during MAD accretion, then the maximum⁷ energy released by the jet prior to time t is given by

$$E(t) \propto \int_{t_{\text{peak}}}^t t'^{-\alpha} dt' = \frac{t_{\text{peak}}^{1-\alpha} - t^{1-\alpha}}{\alpha - 1}, \quad (51)$$

where $\alpha \sim 5/3 - 2.2$. If one demands that the jet energy released before the trigger exceeds the energy released after the trigger,

$$1 < \frac{E(t_{\text{trig}})}{E(\infty) - E(t_{\text{trig}})} = \left(\frac{t_{\text{trig}}}{t_{\text{peak}}} \right)^{\alpha-1} - 1, \quad (52)$$

then this requires

$$t_{\text{trig}} > 2^{1/(\alpha-1)} t_{\text{peak}}. \quad (53)$$

⁷ This is a maximum since we assume that accretion is in a MAD state at all times, such that $P_j \sim \dot{M}c^2$ (eq. [17]). Prior to the onset of MAD (Stage 1 in Fig. 2) the jet efficiency is instead limited by the amount of accumulated magnetic flux (eq. [3]). Also, the jet can be stifled at early times when the magnetic field is dynamically weak ($\phi_{\bullet} < \phi_{\text{on}} \approx 20$) by the high ram pressure of the thick misaligned inflow (Komissarov & Barkov 2009).

Aside from a different prefactor, this constraint is identical to that based on the shape of the X-ray light curve (eq. [11]). Self-consistency of our model thus requires that the off-axis power be similar to that required to explain the observed radio rebrightening.

Although we focus above on energy injected off-axis prior to the γ -ray trigger, this is not the only means by which the jets could inject “invisible” energy into the ambient medium. The onset of MAD accretion after the γ -ray trigger may cause the jet to wobble in and out of our line of sight, giving rise to high amplitude variability (§3.3; Stage 2 in Fig. 2). Since during this process the jets are pointed towards our line of site only a fraction of the time, most of their energy is released during a mis-aligned state. Indeed, the ~ 10 per cent duty cycle of the observed flaring (Fig. 1) suggests that the energy injected during misaligned phases could exceed that injected along our line of site by an order of magnitude. Since $\sim 1/2$ of the total X-ray fluence occurred during the first $t - t_{\text{trig}} \lesssim 10$ days (wobbling jet phase), misaligned jets could produce off axis relativistic ejecta with ~ 5 times more energy than that directly probed by the observed γ -ray/X-ray emission. This alone might be sufficient to power the observed rebrightening, without the need for significant energy injection prior to the trigger.

5.5 Predictions

5.5.1 X-ray Transients

We postulate that Sw J1644+57 resulted from a somewhat special geometric configuration, in which the BH spin axis was pointed along our line of site. This favourable geometry resulted in several bright flares over the first ~ 10 days, which are produced as the jet settles down into its fully aligned configuration (Stage 2 in Fig. 2; § 4.2.1, 5.3). If, however, we had instead been positioned along a more ‘typical’ line of site not aligned with the BH, then we might only have observed a small number of flares, possibly just one in the majority of cases. Such a single flare would appear as an X-ray/soft γ -ray transient of duration $\sim 10^3$ s, yet unaccompanied by an extended luminous X-ray tail as characterized Sw J1644+57.

Could such a population of off-axis jetted TDE flares be contributing to the known population of high energy transients? Given their long duration and low luminosity, such flares could be mistaken for a long-soft gamma-ray burst (GRB) or an X-ray Flash. Perhaps the closest known analog is the class of ‘low-luminosity GRBs’ (LLGRBs) (e.g. Soderberg et al. 2006; Cobb et al. 2006), although most of these are probably not standard TD events due to their locations off the nucleus of their host galaxies and their observed association with core-collapse supernovae (e.g. Chornock et al. 2010; but see Shcherbakov et al. 2012). The volumetric rate of LLGRBs actually exceeds that of classical GRBs (Soderberg et al. 2006), but only a handful are known since they are more challenging to detect than luminous high redshift GRBs (see Nakar & Sari 2012 for a recent compilation). Thus, even if the rate of single-flare off-axis TD jets is a factor of ~ 10 times higher than the rate of Sw J1644+57-like events, it is unclear how many should have been detected yet. If such an event is eventually detected, perhaps by the next generation of wide-field X-ray telescopes, it may be distinguished from normal LLGRBs by its [1] nuclear position; [2] associated optical/UV/soft X-ray emission produced by isotropic thermal emission from the accretion disk or ionized stellar ejecta (Strubbe & Quataert 2011; Clausen et al. 2012), rather than a core-collapse SNe; [3] delayed radio emission from the off-axis jet (Giannios & Metzger 2011; §5.5.3).

5.5.2 Jet Revival

Although the jet in Sw J1644+57 is presently off, our model predicts that the BH continues to accrete through a geometrically-thin accretion disk in a jet-less “thermal state”. However, eventually the mass accretion rate will decrease below $\approx 2\%$ of \dot{M}_{Edd} (Maccarone 2003), after which point the flow may transition to a “hard” state, as characterized by a radiatively-inefficient geometrically-thick accretion flow. Once this transition occurs, magnetic flux can once again accumulate near the black hole on a short timescale ($\sim t_{\text{acc}}$; eq. 42), resulting in a new MAD accretion phase (Stage 5 in Fig. 2). A jet aligned with the Earth and BH spin axis will thus again form, with a power that again tracks the accretion rate \dot{M} . From Figures 5 and 6 we estimate that the X-ray flux will be $\sim 2 \times 10^{-14} - 10^{-13}$ erg cm $^{-2}$ s $^{-1}$ when the jet turns back on, well within the detection limits of current X-ray observatories.

In order to test this idea, we strongly encourage regular X-ray follow-up of Sw J1644+57 over the next decade. The timescale and flux of the observed revival would inform [1] the rate at which the accretion rate is decreasing, and therefore help to distinguish between partial and complete disruption scenarios, or whether the disk has transitioned to a spreading evolution (e.g. Cannizzo et al. 2011) [2] the ratio of accretion rates which characterize the thick \rightarrow thin disk and thin \rightarrow thick disk transitions, respectively; [3] and whether the jet beaming correction (related to the opening angle and bulk Lorentz factor) during the low-hard state are similar to those during the super-Eddington state.

5.5.3 Ubiquity of Radio Transients from TD Events

Due to the enormous energy released in relativistic ejecta, Sw J1644+57 remains a bright radio source ($F_{\nu} \sim 1 - 10$ mJy at $\nu \sim 1 - 50$ GHz) even now, almost two years after the TD event. Since most of the jet activity occurred \sim months around the trigger time, by now the ejecta has slowed down appreciably due to interaction with the circumnuclear medium. The current expansion velocity of the ejecta is at most mildly relativistic $\gamma \sim 2$ (B12), in which case the radio emission should be relatively isotropic (i.e. flux varying by less than an order of magnitude from front to side).

The fact that Sw J1644+57 is a bright isotropic radio source has two implications: First, given the relatively close proximity ($z \sim 0.1$) of most candidate events detected over the past several years, any jet from these events as remotely as powerful as that in Sw J1644+57 should be easily detectable by now, even if the jet remains always pointed away from our line of site. Bower et al. (2012) and van Velzen et al. (2012) have conducted radio follow-up observations of previous thermal TD flares; since most of these observations produced only deep upper limits (with a few interesting exceptions), this already constrains the fraction of TD events accompanied by powerful jets to be $\lesssim 10$ per cent. In hindsight it is perhaps unsurprising that Sw J1644+57 is unique, given the enormous magnetic flux required to power its jet, which could require special conditions not satisfied by most TDs (§5.2; De Colle et al. 2012). A second consequence of the radio luminosity of Sw J1644+57 is that off-axis emission from other jetted TD events (albeit rare) is isotropic and hence should be detectable out to much higher redshifts ($z \sim 1$). Such events are one of the most promising sources for future wide-field radio surveys (Giannios & Metzger 2011; van Velzen et al. 2011; Frail et al. 2012; see Cenko et al. 2012 for a potential high redshift analog to Sw J1644+57), which will help constrain the rate and diversity of jetted TD events.

6 CONCLUSIONS

We have presented a self-consistent model that explains many of the previously disparate puzzles associated with the jetted TD event Sw J1644+57 (Fig. 2; §3). This model relies on just one major assumption: the accumulation of a large, dynamically-important magnetic flux near the central BH, such that the accretion flow from the returning stellar debris becomes magnetically-arrested (MAD; §3.3) on a timescale of \sim week-month after the TD event (Figs. 5–6). The onset of MAD accretion in Sw J1644+57 naturally accounts for (i) the period of intense flaring that lasted for the first \sim 10 days after the trigger; (ii) the approximate constancy (in a time-average sense) of the luminosity during this period; (iii) the subsequent transition of X-ray luminosity to a steady (non-precessing) jet with a power that tracks the predicted power-law decline in the accretion rate; (iv) the sudden shut off of the jet emission at \sim 500 days after the trigger; and (v) the potential origin of the mysterious late-time radio rebrightening that started about a month after the trigger. Our model also naturally predicts a QPO (at a frequency closely tied to that of a BH spin) that is consistent with that seen in the lightcurve of Sw J1644+57.

We emphasize that the strong magnetic flux required by our model is not an entirely independent assumption: a flux of at least this magnitude is necessary to explain the observed jet power in the first place (eq. 3; §5.2; given plausible values of the BH mass and spin), while a much weaker flux would be unable to produce a jet at all (the jet would be ‘stifled’) against the powerful ram pressure of the misaligned disk (Komissarov & Barkov 2009).

ACKNOWLEDGEMENTS

We thank James Guillochon, Michael Kesden, Serguei Komissarov, Julian Krolik, Morgan MacLeod, Jonathan C. McKinney, Petar Mimica, Ramesh Narayan, Ryan O’Leary, Asaf Pe’er, Tsvi Piran, Eliot Quataert, Roman Shcherbakov, Nicholas Stone, and Sjoert van Velzen for insightful discussions. AT was supported by a Princeton Center for Theoretical Science fellowship and an XSEDE allocation TG-AST100040 on NICS Kraken and Nautilus and TACC Ranch.

REFERENCES

Abramowicz M. A., Jaroszyński M., Kato S., et al., 2010, *A&A*, 521, A15
 Beckwith K., Hawley J. F., Krolik J. H., 2008, *ApJ*, 678, 1180
 Berger E., Zauderer A., Pooley G. G., et al., 2012, *ApJ*, 748, 36
 Bloom J. S., Giannios D., Metzger B. D., et al., 2011, *Science*, 333, 203
 Bower G. C., Metzger B. D., Cenko S. B., et al., 2012, *ArXiv:1210.0020*
 Burrows D. N., et al., 2011, *Nature*, 476, 421
 Cannizzo J. K., Troja E., Lodato G., 2011, *ApJ*, 742, 32
 Cao D., Wang X.-Y., 2012, *ApJ*, 761, 111
 Cenko S. B., Krimm H. A., Horesh A., et al., 2012, *ApJ*, 753, 77
 Chabrier G., 2003, *ApJ*, 586, L133
 Chornock R., Berger E., Levesque E. M., et al., 2010, *ArXiv:1004.2262*
 Clausen D., Sigurdsson S., Eracleous M., et al., 2012, *MNRAS*, 424, 1268
 Cobb B. E., Bailyn C. D., van Dokkum P. G., et al., 2006, *ApJ*, 645, L113
 De Colle F., Guillochon J., Naiman J., et al., 2012, *ApJ*, 760, 103
 Fender R. P., et al., 2004, *MNRAS*, 355, 1105
 Fragile P. C., Blaes O. M., Anninos P., Salmonson J. D., 2007, *ApJ*, 668, 417
 Frail D. A., Kulkarni S. R., Ofek E. O., et al., 2012, *ApJ*, 747, 70
 Giannios D., Metzger B. D., 2011, *MNRAS*, 416, 2102
 Greene J. E., 2012, *arXiv:1211.7082*
 Guillochon J., Ramirez-Ruiz E., 2012, *ArXiv e-prints*

Haas R., Shcherbakov R. V., Bode T., Laguna P., 2012, *ApJ*, 749, 117
 Igumenshchev I. V., 2008, *ApJ*, 677, 317
 Kepler S. O., Pelisoli I., Jordan S., et al., 2012, *ArXiv:1211.5709*
 Kesden M., 2012, *Phys. Rev. D*, 85, 024037
 Komissarov S. S., Barkov M. V., 2009, *MNRAS*, 397, 1153
 Krimm H. A., Barthelmy S. D., 2011, *GRB Coordinates Network*, 11891, 1
 Krolik J. H., Piran T., 2011, *ApJ*, 743, 134
 Krolik J. H., Piran T., 2012, *ApJ*, 749, 92
 Lei W.-H., Zhang B., Gao H., 2012, *ArXiv:1202.4231*
 Levan A. J., Tanvir N. R., Cenko S. B., et al., 2011, *Science*, 333, 199
 Liu D., Pe’er A., Loeb A., 2012, *ArXiv:1211.5120*
 Lodato G., King A. R., Pringle J. E., 2009, *MNRAS*, 392, 332
 Maccarone T. J., 2003, *A&A*, 409, 697
 MacLeod M., Guillochon J., Ramirez-Ruiz E., 2012, *ApJ*, 757, 134
 McKinney J. C., Blandford R. D., 2009, *MNRAS*, 394, L126
 McKinney J. C., Tchekhovskoy A., Blandford R. D., 2012a, *Science*, doi:10.1126/science.1230811
 McKinney J. C., Tchekhovskoy A., Blandford R. D., 2012b, *MNRAS*, 423, 3083
 Metzger B. D., Giannios D., Mimica P., 2012, *MNRAS*, 420, 3528
 Nakar E., Sari R., 2012, *ApJ*, 747, 88
 Narayan R., et al., 2003, *PASJ*, 55, L69
 Narayan R., Yi I., 1995, *ApJ*, 444, 231
 Ohsuga K., Mori M., Nakamoto T., Mineshige S., 2005, *ApJ*, 628, 368
 Panaitescu A., Kumar P., 2002, *ApJ*, 571, 779
 Phinney E. S., 1982, *MNRAS*, 198, 1109
 Rees M. J., 1988, *Nature*, 333, 523
 Rees M. J., Begelman M. C., Blandford R. D., et al., 1982, *Nature*, 295, 17
 Reis R. C., et al., 2012, *Science*, 337, 949
 Russell D. M., Miller-Jones J. C. A., Maccarone T. J., et al., 2011, *ApJ*, 739, L19
 Saxton C. J., Soria R., Wu K., Kuin N. P. M., 2012, *MNRAS*, 422, 1625
 Sbarufatti B., Burrows D. N., Gehrels N., et al., 2012, *The Astronomer’s Telegram*, 4398, 1
 Shcherbakov R. V., Pe’er A., Reynolds C. S., et al., 2012, *ArXiv:1212.4837*
 Socrates A., 2012, *ApJ*, 756, L1
 Soderberg A. M., Kulkarni S. R., Nakar E., et al., 2006, *Nature*, 442, 1014
 Steiner J. F., McClintock J. E., Remillard R. A., et al., 2010, *ApJ*, 718, L117
 Steiner J. F., Narayan R., McClintock J. E., et al., 2009, *PASP*, 121, 1279
 Stone N., Loeb A., 2012, *Physical Review Letters*, 108, 061302
 Stone N., Sari R., Loeb A., 2012, *ArXiv e-prints*
 Strubbe L. E., Quataert E., 2009, *MNRAS*, 400, 2070
 Strubbe L. E., Quataert E., 2011, *MNRAS*, 415, 168
 Tchekhovskoy A., McKinney J. C., 2012a, *MNRAS*, in preparation
 Tchekhovskoy A., McKinney J. C., 2012b, *MNRAS*, 423, L55
 Tchekhovskoy A., McKinney J. C., Narayan R., 2012, *JPCS*, 372, 012040
 Tchekhovskoy A., Narayan R., McKinney J. C., 2010, *ApJ*, 711, 50
 Tchekhovskoy A., Narayan R., McKinney J. C., 2011, *MNRAS*, 418, L79
 Ulmer A., 1999, *ApJ*, 514, 180
 van Velzen S., Frail D. A., Koerding E., Falcke H., 2012, *ArXiv:1210.0022*
 van Velzen S., Körding E., Falcke H., 2011, *MNRAS*, 417, L51
 Wiersema K., van der Horst A. J., Levan A. J., et al., 2012, *MNRAS*, 421, 1942
 Zauderer B. A., Berger E., Margutti R., others. 2012, *ArXiv:1212.1173*
 Zauderer B. A., Berger E., Soderberg A. M., et al., 2011, *Nature*, 476, 425